CHALMERS
UNIVERSITY OF TECHNOLOGY

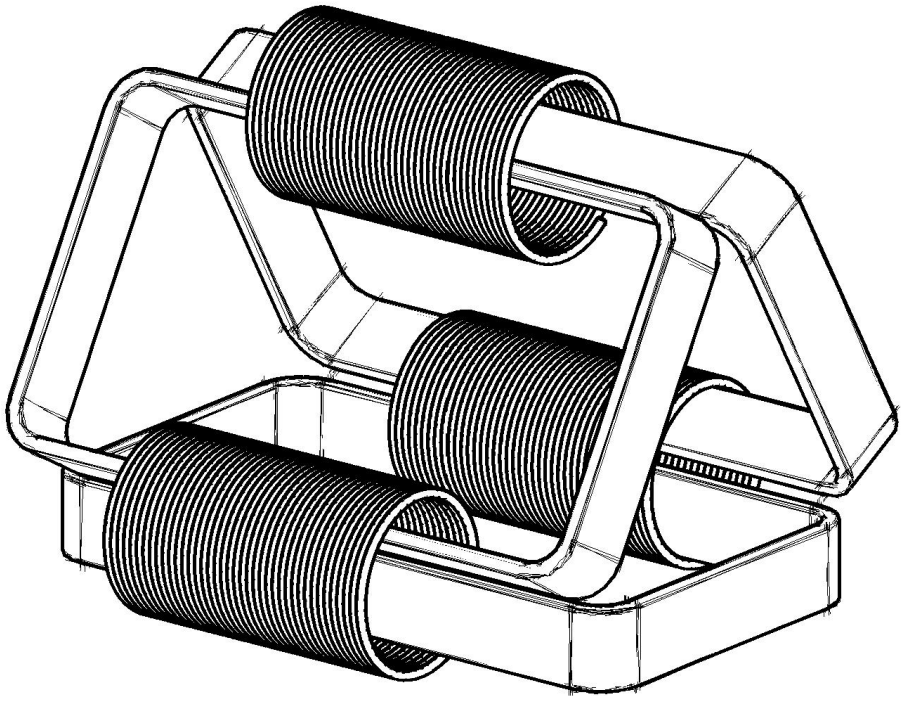

Effect of magnetic bypass on performance of hexa-core distribution transformer

Master's thesis in Electrical Power Engineering

Lorand Gergely
Jeff Antony Ukken

Department of Electrical Engineering
CHALMERS UNIVERSITY OF TECHNOLOGY
Gothenburg, Sweden 2018

Master of Science Thesis

Effect of magnetic bypass on performance of hexa-core distribution transformer

Lorand Gergely - Jeff Antony Ukken

CHALMERS
UNIVERSITY OF TECHNOLOGY

Department of Electrical Engineering
Chalmers University of Technology
Gothenburg, Sweden 2018

Effect of magnetic bypass on performance of hexa-core distribution transformer
LORAND GERGELY, JEFF ANTONY UKKEN

Supervisor: Thomas Türk, Transformer Cage Core AB
Examiner: Yuriy Serdyuk, Department of Electrical Engineering, Chalmers University of Technology

Master's Thesis
Department of Electrical Engineering
Chalmers University of Technology
SE-412 96 Gothenburg
Telephone +46 31 772 1000

Gothenburg, Sweden 2018

Effect of magnetic bypass on performance of hexa-core distribution transformer
Lorand Gergely, Jeff Antony Ukken

Abstract

The amount of distribution transformers in service increases in the expanding power distribution system and the total no-load power loss in the transformers become significant. There are already restrictions by the EU Commission on no-load loss for new transformers and new requirements for their further reduction by 10% are expected by 2021.
In this thesis, a prototype of a hexa-transformer core was used to validate and check the effect of bypass on no-load loss reduction. The design of the yoke of the core, was modified to incorporate gaps between each layer to include the bypasses.
Four different bypass configurations were studied, namely single, two and three step grain oriented steel bypass as well as one step non-grain oriented steel bypass. These configurations implemented various turning angles of the magnetic flux through the bypass.
As the result, a loss decrease of $\approx 15\%$ to $\approx 19.5\%$ in a single step,$\approx 17\%$ to $\approx 24\%$ in two step, $\approx 14\%$ to $\approx 26\%$ in three step grain oriented steel and $\approx 3\%$ to $\approx 13\%$ in non-grain oriented steel was measured depending on the level of magnetic induction.
It is shown that this reduction of loss is achieved due to the decrease of the magnetic flux in the core rings. The single step grain oriented steel bypass demonstrated the highest magnetic flux in the bypass and least iron added to the core that make it the most optimal solution among the studied cases.

Keywords: hexa-transformer, transformer losses, magnetic bypass, transformer design,bypass, single step bypass, two step bypass, three step bypass

Acknowledgements

The authors would like to express their sincere gratitude towards Yuriy Serdyuk, supervisor and examiner for this project, for his continuous support and guidance throughout the study. His dedication and expertise have helped us greatly in successful completion of the project.
Furthermore, the authors would also like to thank Thomas Türk, supervisor at Transformer Cage Core AB, for his support, motivation and guidance all along the project. His experience with project has helped us abundantly in following the right path throughout the study.
The authors are also grateful towards Ehsan Bahmani and Sima Soltanipour for their valuable comments and suggestions on the project. Appreciation is also given to everyone at Transformer Cage Core AB and Division of Electric Power Engineering at Chalmers University of Technology, who have helped with time and expertise throughout the project.
Last but not least, the authors would also like to thank their family and friends for their love and support all through out.

Lorand Gergely - Jeff Antony Ukken,

Gothenburg, June, 2018

Contents

List of Figures

List of Tables

1

Introduction

1.1 Background

The energy industry grows with more demand of power based on industrial growth. The total energy consumption in Europe has been increased by 25% over past 25 years with annual increase of 2.5%.[1]. With increase in power requirements the transmission and distribution system also enlarges. One of the major components on a distribution system is distribution transformers.

A distribution transformer is used close to the end user (industrial and domestic) to step-down voltage to user specific levels. Depending on the type of user, like a domestic user or small industry, the distribution transformer is not always on load. Being an unavoidable part in the transmission system, the losses from the transformer are considered crucial.As pointed out in [2], the total power losses from distribution transformers account for 33.4TWh/year of which 63% are no-load losses.

According to the EU Comission this power loss in the transformers is equal with the half of the total energy production of Denmark in the EU. Since power generation stands for one third of the CO_2 emission, a regulation already has been taken place, in order to meet the emission target set by the EU. These regulations are aimed to force the transformer manufacturer to decrease the transformer no-load power loss by 20%. This regulation was divided into two stage, each stage contains a 10% decrease of power loss in the transformers. The first stage was validate 2015 and the next step is planned to be validate by 2021 [3].

The losses in the transformers are the copper loss in the windings and the iron loss (hysteresis and eddy current) in the core, in other words the heat generated by the winding and the core. A solution to reduce these losses is to increase the iron content of the core legs. However increasing the iron content in the core, changes the dimension of the core demanding more copper to be added which increases the total cost of materials of the transformer core itself. On the other hand, another option is to reduce the losses within the core by improving the design of transformer core.

1.2 Problem description

To evaluate the effect of the bypass on no-load losses the magnetic induction has to be studied. This is due to the fact that the no-load loss is proportional to the square of the magnetic induction(B^2). As it is known the magnetic induction is proportional to the magnetic flux and inverse proportional to the cross section area. Therefore, a theoretical approach will be based on the magnetic flux to understand the effect of the bypass.

The practical part of this project is to measure the above mentioned magnetic flux and the no-load losses. To measure the magnetic flux a search coil with an integrator will be used. The search coil working principle is based on the Faraday's law of induction, which states that the induced voltage across an N turns of wire is equal with the product of the number of turns and the negative time rate change of the magnetic flux. The voltage across the integrator will give the magnetic flux. Moreover,the no-load loss will be measured with a watt-meter.

Beside solving the task mentioned above, a comparison between the different bypass configurations will be made. This project will try to choose the most optimal solution between the bypass configurations based on sustainable and loss reduction perspective.

1.3 Aim

The aim of this thesis is to present the effect of a bypass in a hexa-transformer core in terms of no-load losses. Furthermore, the project also focuses on comparison between four different types of bypass configuration and find an optimal solution between the amount of added steel and the loss reduction.

1.4 Scope and limitations

This project deals with a comparison between four different type of bypass configurations and trying to find an optimal solution between them. Since, the measurement is done on a down-scaled laboratory core, which physical state is unknown, as well it contains different number of layer in the core rings, the harmonics contain for the measured magnetic flux will be not studied and compared.

For the practical part, the windings will be made by hand, which can result in a non uniformity and can cause an error in the excitation and measurement. As it was mentioned above, the core rings contains different steel layer and there is an asymmetry between the phases. Moreover, the bypass pieces have to be inserted by hand in the core. This handling can result in damage to the annealed section, which might increase the loss. Furthermore, due to the ferromagnetic material characteristics in the non-linear region it makes hard to measure the loss at the same excitation level. Therefore, the measured loss data will be interpolated in

order to have a good comparison between the different bypass configuration loss curves.
In additional, the non-grain oriented steel has a much higher rated loss than the grain oriented steel. However, the comparison will be made based on the measurement.

1.5 Ethics

In this project the IEEE code of ethics and guidelines have been followed. The following text discuss the issues that is important of this project.

First, it is important to mention the safety aspect. The connection between the core and the generator was made with respect to safety standards, i.e there was no naked wire around the connection that can cause personal injury. However, it is advised to keep a safety distance when the system is on operation. Moreover, the bypass pieces has to be mounted with hands to the core. For this reason, it is important to make a routine, which can eliminate the possibility that the core is being touched when the system is live.

Finally, the comparison is made by considering the magnitude of the magnetic flux in the bypass, the cross section area and the loss reduction. However, the bypass pieces has different dimensions, which makes it impossible to have the same cross section area, stress and the same bypass placement across the core. As it was observed, higher cross section area between two slots increased the stress to the core and the loss has increased. Moreover, there is a possibility that during the mounting of the bypass pieces, different layers have been bypassed causing more asymmetric between core ring phases.

2

Theory

Transformers are static electrical machines which are used to change the voltage or current of a given transmission point keeping the power transferred unchanged [5]. They are used from low power applications which include household appliances to large power transmission units. Based on the power ratings the power transformers are generally classified as transmission transformers and distribution transformers. The distribution transformers are those which are in the customer end of transmission network. On a regular day, the loaded hours for these transformers are much lower compared to the transmission side transformers. A greater percentage of losses accounted from these transformers are from core losses.

This chapter focuses on the basic working principle of a power transformer and the losses within the transformer. Furthermore, the chapter also focuses on basic principles behind a hexa-transformer and the effect of the bypass on reducing the no-load losses.

2.1 Transformer working principle

A simple transformer consist of two separate windings connected with a core. The core of a transformer is a magnetic material, normally laminated sheets to reduce the eddy currents within the core. Figure 2.1 shows a basic transformer setup where V_p, I_p, and N_p are voltage across the input terminals, primary side current and number of turns in the primary side respectively. V_s, I_s and N_s are the respective quantities on secondary side.

The working principle is based on Faraday's law of induction. An AC input voltage is applied at the primary side, which induce magnetic flux in the core. The electrical energy is converted to magnetic energy, afterwards it is reconverted to electrical energy. The mutual inductance between both the coils is very high, so that the flux leakage is minimized [6].

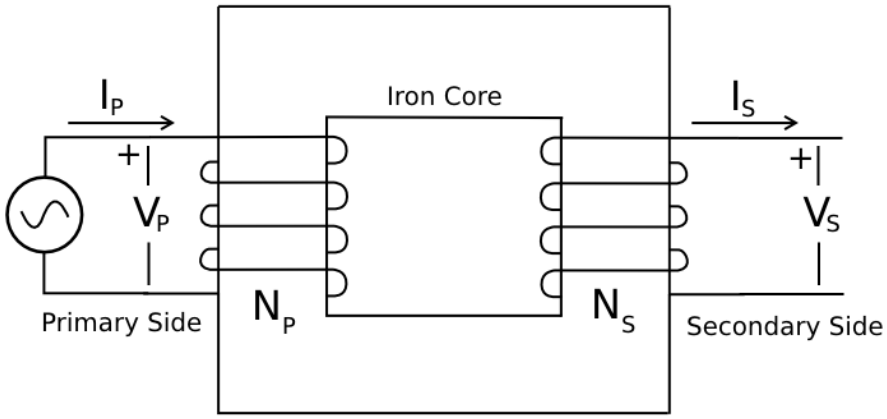

Figure 2.1: Basic transformer circuit

From Faraday's laws of electromagnetic induction, the induced voltage in the secondary windings can be written as

$$V_s = -N_S \frac{d\phi_m}{dt}, \tag{2.1}$$

where ϕ_m is the flux linked with the secondary coil at a given time. The rated applied voltage on the primary side of the transformer is given by

$$V_p = 4.44 f N_P B_m A, \tag{2.2}$$

where f is the frequency of the time varying field, B_m the flux density in the core and A the area of cross-section of the iron. For a given distribution system, magnitude of frequency remains constant. Thus the above equation can be simplified to

$$V_p \propto N_P B_m A. \tag{2.3}$$

Increasing the flux density in the core reduces the dimension of the core as such, too high induction saturates the core iron. This increases the losses and distorts the secondary voltage. The normal operating range of a power transformer made by a grain-oriented electrical steel is between 1.5T to 1.7T.

2.1.1 Ferromagnetic materials

Ferromagnetic materials exhibit long range ordering, where the electron spins in atomic level align to form domains. Figure 2.2 shows how the domains are aligned in a ferromagnetic material. When placed in a magnetic field the domains align in the direction of field to have most flux flowing through the material volume. [4].

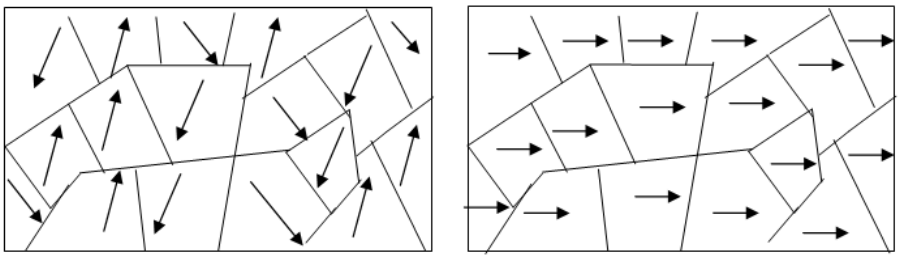

Figure 2.2: Magnetic domains in a ferromagnetic material before and after application of magnetic field

For a transformer core, an improved version of this ferromagnetic material is used to reduce the losses. The steel is grain oriented to have the flux in one plane, as in a transformer the flux flows only in two directions. The losses in grain oriented steel are much lower than in non-grain oriented steel.

2.2 Losses in a transformer

The losses in transformer are given as a sum of core, copper, dielectric and stray losses. The core losses are given as the sum of hysteresis losses and eddy current losses. The stray losses in the transformer is negligible when there is no load. Also the magnitude of dielectric losses in the no-load losses is very small with respect to hysteresis and eddy current losses [7]. Figure 2.3 shows a representation of how the total losses in a transformer are subdivided.

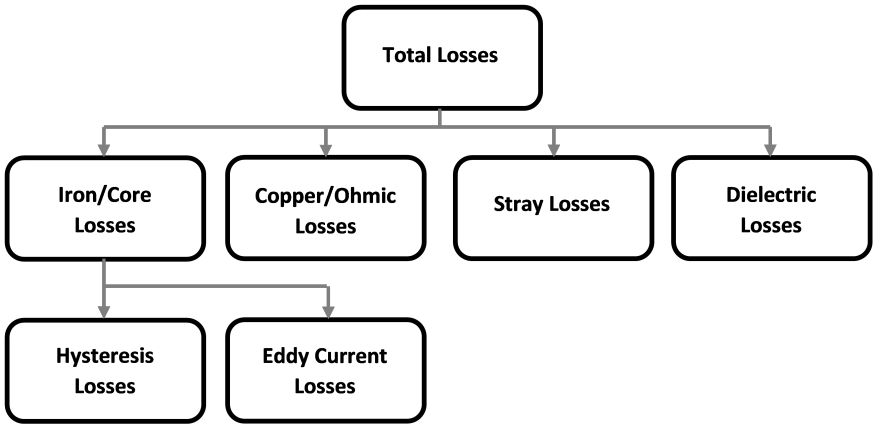

Figure 2.3: Loss division in a transformer

2.2.1 Hysteresis losses

The alternating field produced by the source in the ferromagnetic material incurs loss in the core material due to the hysteresis effect. During the magnetization, the atomic domain align along the applied magnetic field, however during the demagnetization the atomic domain remains aligned even when there is no magnetic field

across the material. Hence, during the demagnetization and re-magnetization the magnetization curve does not follow the initial magnetization curve, as it shows in Figure 2.4.

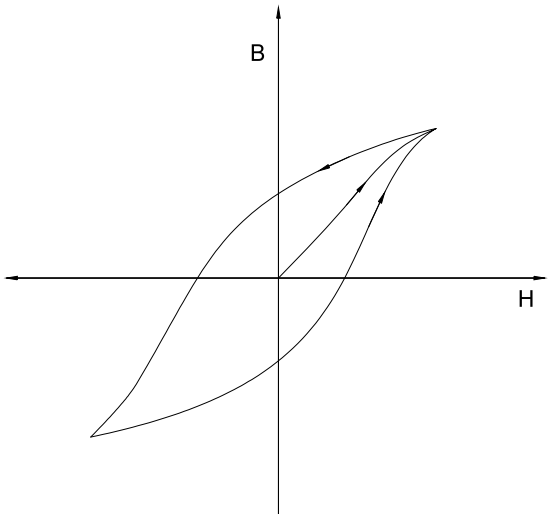

Figure 2.4: Illustration of a hysteresis loop for a ferromagnetic material

The hysteresis loss can be calculated as:

$$P_h = k_h f B_m^{\beta}, \tag{2.4}$$

where k_h is the hysteresis coefficient. The loss is proportional to β(normally around 2) power of B_m [8].

2.2.2 Eddy current losses

The core magnetic material in the transformer is a conductor. When subjected to alternating fluxes, an emf is induced within the volume of the core resulting in circulating currents. These currents add on to the losses in the core. These losses are reduced by making the core out of thin laminated sheets. The magnitude of these losses are given by the equation:

$$P_e = k_e (f B_m)^2, \tag{2.5}$$

where k_e is the eddy current coefficient and f the frequency of the primary AC source [8].
From the above two loss equations the core losses are solely dependent on flux density in the core for a given frequency. Reduction of flux density in the core reduce the net core losses. The flux density in the core is given by

$$B = \frac{\phi}{A}, \tag{2.6}$$

where B is the flux density, ϕ is the magnetic flux and A the area of the cross-section of the core.

2.2.3 Copper losses

The copper loss is due to the heat caused by the current through the copper windings. According to Joule first law, the power loss caused by heat is proportional to the product of the copper resistance and the square of the current. The total copper loss in the transformer can be written as

$$P_{Cu} = 3\ I_p^2 R_{Cu}, \tag{2.7}$$

where I is the current and R_{cu} is the resistance of copper for each phase.

2.3 Hexa-transformers

Hexa-transformer is a 3 phase transformer, which belongs to the symmetrical cage core type family. The shape of the core is a triangle in a top view, having three phases on three legs. The core is built by winding the core steel rather than traditional stacked core. the name of the transformer comes from the cross-section of the transformer leg which is in the shape of a hexagon. It is made by nine different rings arranged in a specific pattern as shown in Figure 2.6. The actual core of a hexa-transformer on a 3D perspective shows in Figure 2.5

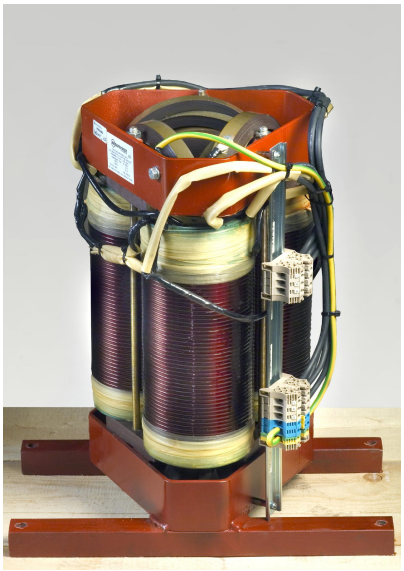

Figure 2.5: Hexa-transformer. Image from [10]

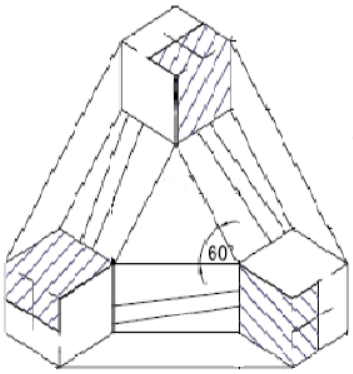

Figure 2.6: Hexa-transformer cross-section. Image from [9]

Due to the symmetry in the core based on the physical shape, and the reluctance being equal in all the paths, the current required to magnetize the core is lower for the same power level of E-type transformer. Compared with a traditional stacked core E-type transformer of same power rating, the hexaformer has higher efficiency and less weight [9].

2.4 Magnetic induction

The losses in consideration being the core losses, which is approximately proportional to the magnetic induction power of two (B^2). According to equation 2.6 the magnetic induction is proportional to the magnetic flux (ϕ) and inverse proportional to the cross-section area (A). Therefore, the following subsections detail on different flux calculations. Furthermore, in order to achieve the desired flux magnitude in the bypass an area calculation is done, as well as a no-load loss calculation will be presented.

2.4.1 Flux in yokes

The flux magnitude in the yoke can be calculated with a vector diagram. Figure 2.7 shows the vector diagram for three phases. The notation for the flux in the leg are $\vec{\phi_{A_L}}, \vec{\phi_{B_L}}, \vec{\phi_{C_L}}$ and in the core rings $\vec{\phi_{A_1}}, \vec{\phi_{A_2}}, \vec{\phi_{B_1}}, \vec{\phi_{B_2}}, \vec{\phi_{C_1}}, \vec{\phi_{C_2}}$ as it shown in Figure 2.7.

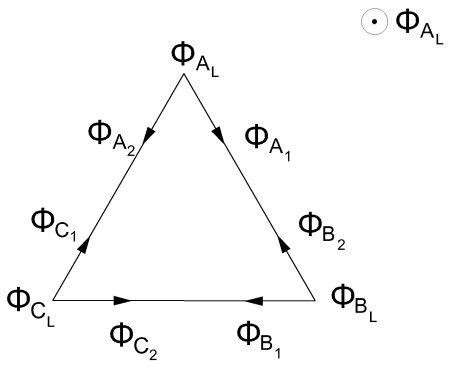

Figure 2.7: Top view vector representation of the core

The sum of the two flux vectors in the core rings has to be equal with the corresponding flux in the leg, according to Kirchhoff's current law. To put in mathematical form it follows

$$\vec{\phi_{A_L}} = \vec{\phi_{A_1}} + \vec{\phi_{A_2}} \tag{2.8}$$

$$\vec{\phi_{B_L}} = \vec{\phi_{B_1}} + \vec{\phi_{B_2}} \tag{2.9}$$

$$\vec{\phi_{C_L}} = \vec{\phi_{C_1}} + \vec{\phi_{C_2}}, \tag{2.10}$$

where $\phi_{A_1} = -\phi_{B_2}$, $\phi_{A_2} = -\phi_{C_1}$ and $\phi_{C_2} = -\phi_{B_1}$. The core rings flux vectors are given by the difference between the two linked leg vectors. This results a 30° angle between the flux in the leg and flux in the core ring. Consequently, the magnitude of the flux in the yoke can be calculated as

$$|\phi_{A_1}| = \frac{|\phi_{A_L}|}{\sqrt{3}}. \tag{2.11}$$

The resultant vectors in the core rings and the different legs are shown in Figure 2.8, where the 30° angle shift is noted as α. As it can be noticed, since $\phi_{A_2} = -\phi_{B_2}$ it follows that $sin(\alpha) = sin(120 + \alpha)$.

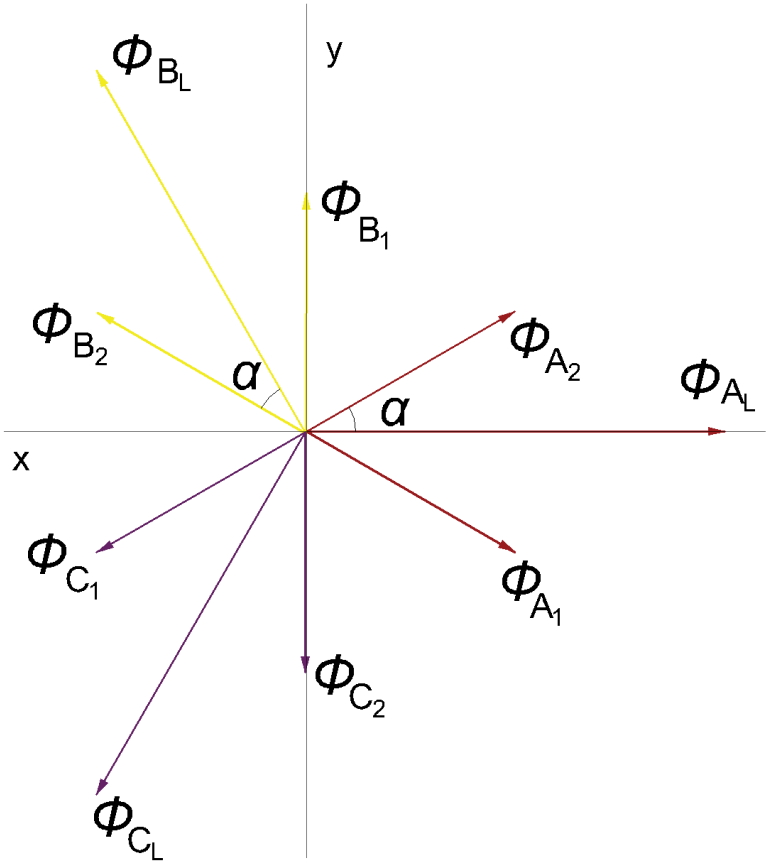

Figure 2.8: Resultant vector representation

2.4.2 Flux in yokes with addition of bypass

By introducing bypass in the yoke, new flux path will be added to the yoke, enabling a flux share between the core rings.

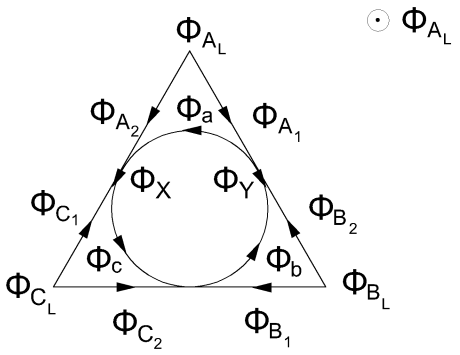

Figure 2.9: Top view vector representation of the core after introducing the bypass

Applying Kirchoff's current law to the circuit shown in Figure 2.9 the following equations can be obtained

$$\vec{\phi_{A_2}} + \vec{\phi_{C_1}} + \vec{\phi_a} = \vec{\phi_c} \tag{2.12}$$
$$\vec{\phi_{A_1}} + \vec{\phi_{B_2}} + \vec{\phi_b} = \vec{\phi_a} \tag{2.13}$$
$$\vec{\phi_{C_2}} + \vec{\phi_{B_1}} + \vec{\phi_c} = \vec{\phi_b}. \tag{2.14}$$

Solving for phase A, it yields:

$$\vec{\phi_{A_2}} = \vec{\phi_c} - \vec{\phi_{C_1}} - \vec{\phi_a} \tag{2.15}$$
$$\vec{\phi_{A_1}} = \vec{\phi_a} - \vec{\phi_{B_2}} - \vec{\phi_b}. \tag{2.16}$$

Figure 2.10 shows the resulting vector diagram. It should be noticed that the most effective way to reduce angle α is when the bypass magnetic flux vector $(\vec{\phi_a}, \vec{\phi_b}, \vec{\phi_c})$ is perpendicular to the corresponding magnetic flux vector in the leg $(\vec{\phi_{A_L}}, \vec{\phi_{B_L}}, \vec{\phi_{C_L}})$. This will always be the case when the flux vectors are symmetric. Furthermore,as angle α decreases consequently the magnitude of flux in the core rings($|\phi_{A_2}|$,$|\phi_{A_1}|$ etc.) decreases with $\Delta\phi_{A_2}$ as it shows in the figure. Moreover, it can be noticed that no matter of the flux magnitude in the bypass, the flux magnitude ϕ_X and ϕ_Y will always be 0.577 p.u and a 30° phase shift.

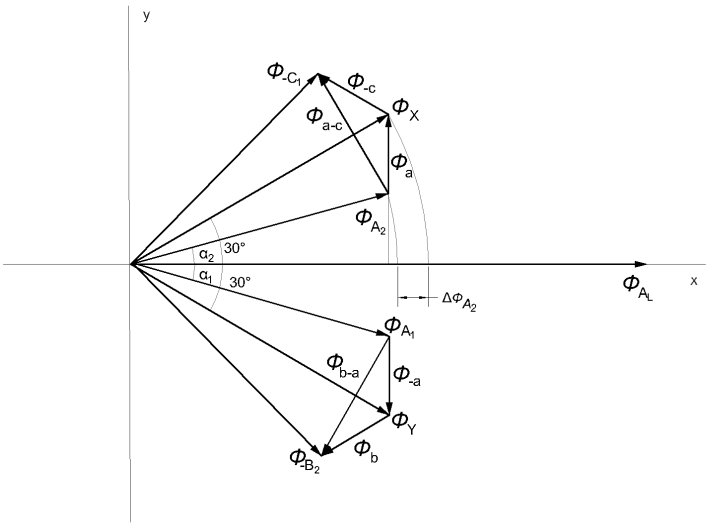

Figure 2.10: Reduction of flux magnitude in the core rings with introduction of bypass

By applying vector algebra the following relations can be obtained:

$$|\phi_{A_1}| = |\phi_{A_2}| = \frac{|\phi_{A_L}|}{2\cos\alpha} \tag{2.17}$$

$$|\phi_a| = \frac{|\phi_{A_L}|\sin(30-\alpha)}{\sqrt{3}\cos\alpha}. \tag{2.18}$$

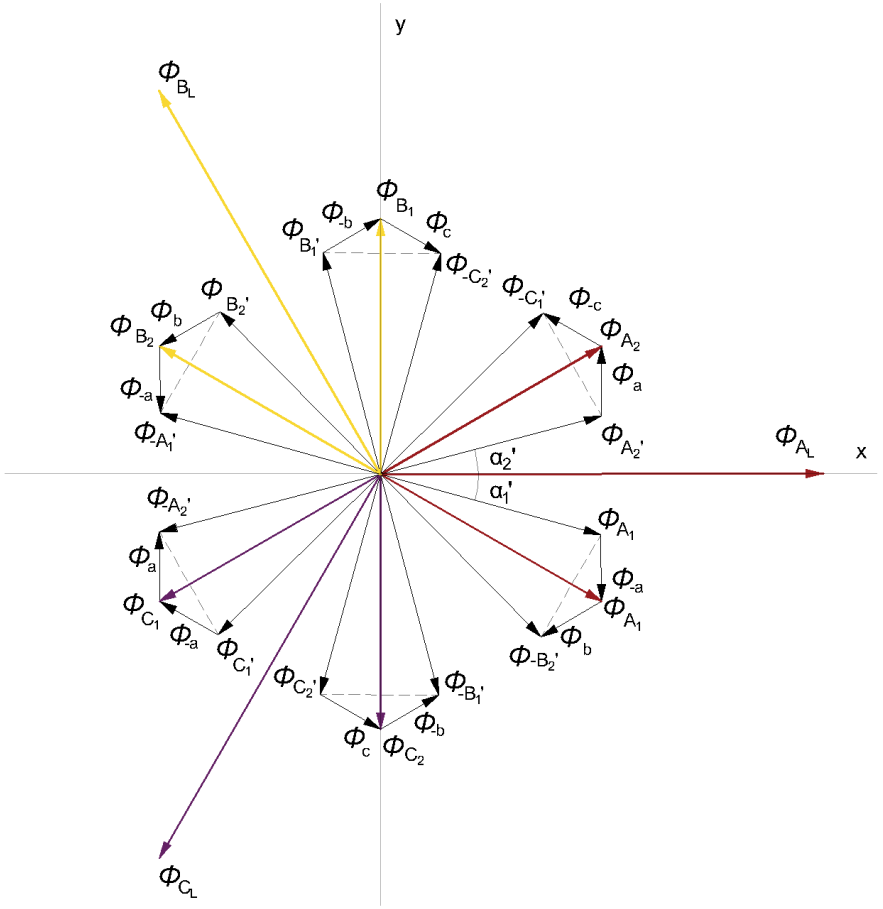

Figure 2.11: Vector diagram with bypass in the core

Figure 2.11 shows the vector diagram for all the three phases. Additionally, Table 2.1 shows the calculated flux vector magnitude values for different angle α, where the leg magnetic flux(ϕ_{A_L}) is normalized to 1 p.u. As it can be observed, the influence

α	$\lvert\phi_{A_2}\rvert$	$\lvert\phi_{C_1}\rvert$	$\lvert\phi_a\rvert$	$\lvert\phi_c\rvert$
30	0.577	0.577	0	0
25	0.551	0.551	0.0555	0.0555
20	0.532	0.532	0.1067	0.1067
15	0.517	0.517	0.154	0.154
10	0.507	0.507	0.2	0.2
0	0.5	0.5	0.2886	0.2886

Table 2.1: Flux magnitude change with different angle α in the yoke and bypass

of angle α on the flux magnitude in the core ring (ϕ_{A_2}) between 10° and 0° is around 1.3% in contrast with almost a 30% increase of flux through the bypass(ϕ_a). This phenomena is illustrated in Figure 2.12.

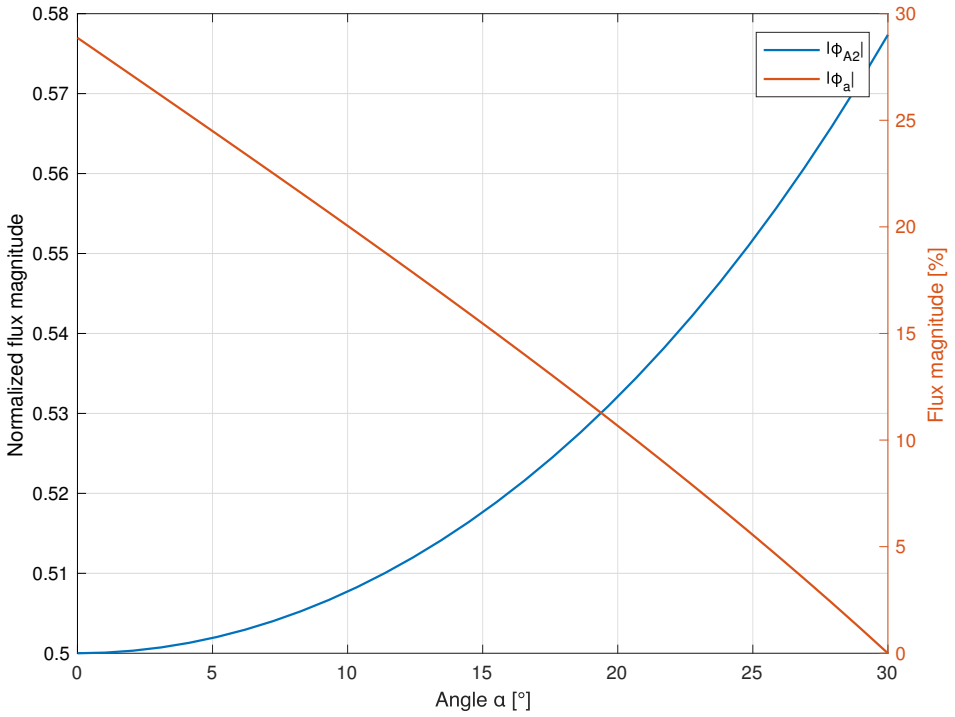

Figure 2.12: Flux change in the core rings and in the bypass with different angle α.

2.4.3 Cross-section area

One way to control and achieve the desired magnetic flux magnitude through the bypass is to consider the cross-section area of the introduced bypass. The following engineering assumption is made to dimension the cross-section area. Assuming that the magnetic induction (B) is fixed in the core and the relation between the magnetic flux and cross-section area is linear, the required cross-section area for the bypass to achieve a 28% of ϕ_{A_L} flux will result a bypass cross-section area of 28% of the cross-section area of the leg.

2.5 Theoretical loss calculation without consideration of the loss in the bypass

In order to estimate the theoretical no-load loss with and without bypass, it is important to have the core material characteristic provided by the manufacturer. These data are measured under an ideal condition, for example low lamination stress, pure sinusoidal flux etc. and it is the absolute minimum loss per kg that can be expected. Additionally, the provided data contains the core losses, hysteresis and eddy current losses for two different frequency, namely 50 Hz and 60 Hz. The magnetic induction in the core rings (B_y) can be calculated by combining equations

2.6 and 2.17

$$B_y = \frac{B_L}{cos(\alpha)}, \tag{2.19}$$

where B_L is the magnetic induction in the leg and α is the phase angle between the flux in the leg and the flux in the rings. The core loss curve for different values of α can be obtained by using equation 2.19 and the given manufacturer loss data. The loss values are taken at magnetic induction level B_y. In case when at magnitude B_y there is no specified loss values it is assumed that between two given magnetic induction level provided by the manufacturer, the loss curve is changing according to the following equation

$$P_{nom.loss}[W/kg] = k\ B_y^n, \tag{2.20}$$

where k is a constant and n is the power factor. By using two magnetic induction level and the corresponding given power loss values by the manufacture, n can be calculated. In this calculation the loss in the bypass is not considered. Figure 2.13 shows the resulting theoretical loss curve based on M103-27P steel type core loss data. The loss values around hard saturation region is assumed to be equal to the maximum rated loss, in this case 2 W/kg.

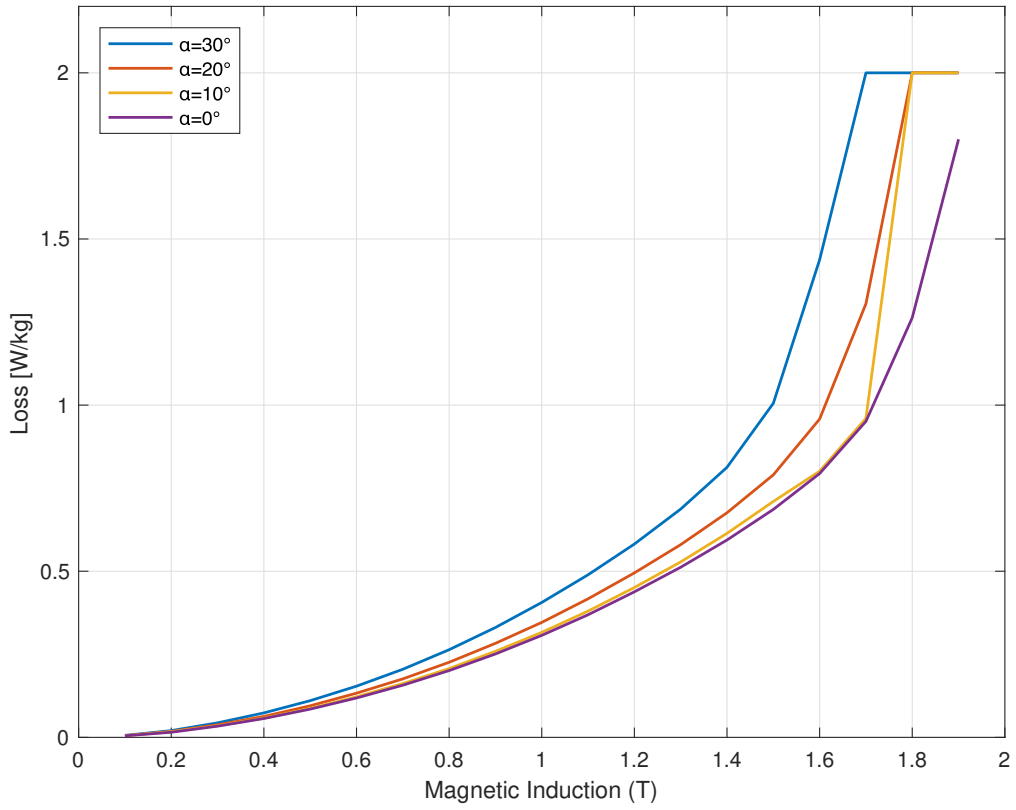

Figure 2.13: Theoretical loss (W/kg) calculation for different angle α without consideration of the loss in bypass.

It should be noticed that in case of $\alpha = 0°$ the power loss is equal to the nominal loss,

i.e to power loss specified by the manufacturer, and in case of $\alpha = 30°$ is reference loss, i.e without bypass. Figure 2.14 shows the loss difference in percentage between the loss curve without bypass and for different angle α.

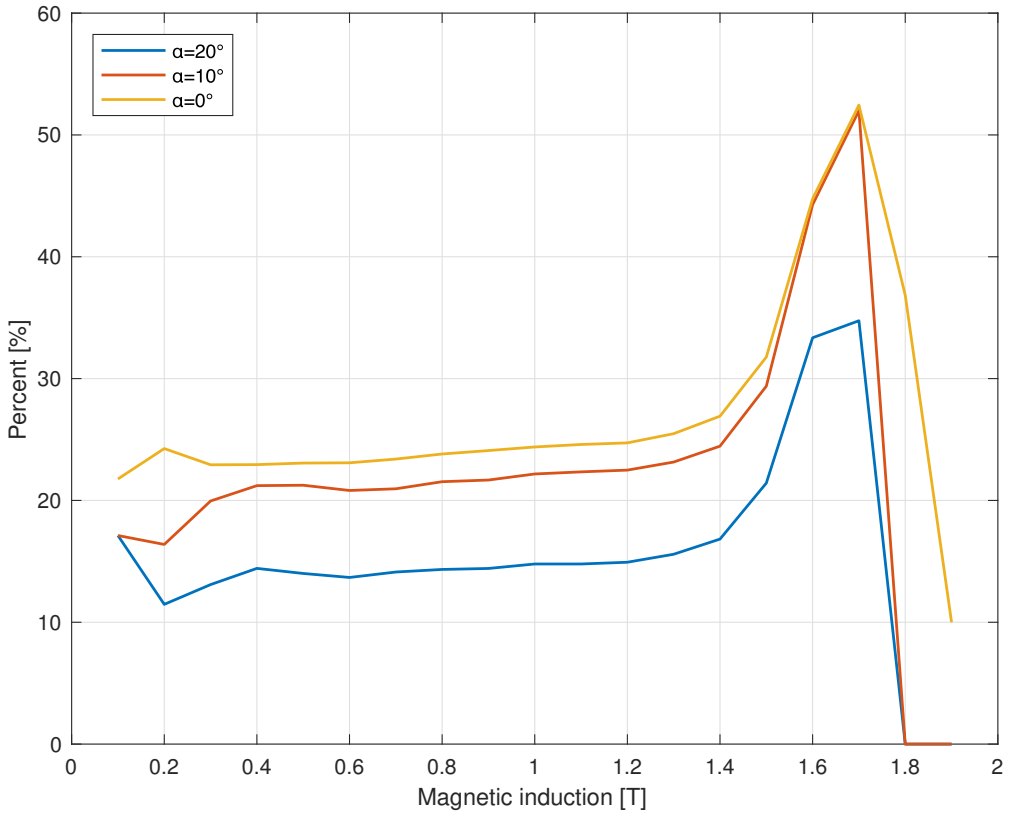

Figure 2.14: The difference in percentage between the loss curve without bypass and for different angle α.

3

Types of bypasses

As the study is focused on the analysis of loss improvement using a bypass, the construction and design of bypass units in the core plays an important role.

When going deep into the yoke structure, the flux flowing through the bypass is required to take a turn of 120 degrees between the yokes. With this constraint taken into consideration, the flux linked between the yokes through the bypass vary with respect to the change in angle and the number of turns the flux take [11]. The design of different types of bypass are detailed in the latter part of this chapter.

3.1 Single step bypass

A single piece of bypass is created to have a link between the yokes. The bypass gives two angle shifts for the flux between the yokes, each of 60°. Figure 3.1 shows an illustration of how the bypass is setup in the core. The deviation on how the flux flows within the bypass is also illustrated on the figure. The bypass is designed for both grain oriented steel and non-grain oriented steel. The non-grain oriented steel has a width of 30 *mm* and a thickness of 0.5 *mm*, in contrast with a $\approx$ 70 *mm* width and 0.23 *mm* thick grain oriented steel.

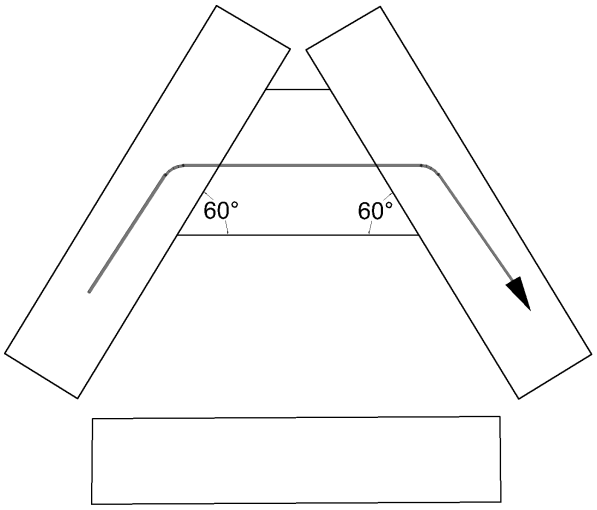

Figure 3.1: An illustration of how a single step bypass is added to the core

3.2 Two step bypass

Two different grain oriented strips are used in this type of bypass to make the link between the yokes. The strips have an angle of 40° on the contact point between yoke and strip and the contact between the strips as it shows in Figure 3.2. In this type of configuration the flux takes the 120° turn in 3 steps of 40°each. The bypass width for the area of cross-section of the bypass is calculated with the minimum width of the bypass. The grain oriented strips have a width of 50 *mm* and a thickness of 0.23 *mm*.

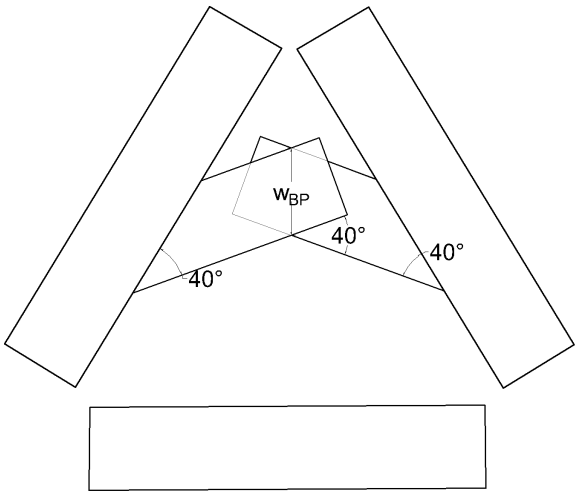

Figure 3.2: An illustration of how a two step bypass is added to the core

3.3 Three step bypass

This bypass configuration is setup by two grain oriented steel strips connected to each of the yoke and grain oriented triangular piece between the two strips. The triangular piece connects the strips to make the link. The strips are placed at an angle of 20° with the yokes and the triangular central piece makes an angle of 40° with the strips, as it shows in Figure 3.3. In this configuration the flux through the bypass needs to make four different turns with two 20 turns and two 40° turns. This type of grain oriented steel has a width of 40 *mm* and a thickness of 0.23 *mm*.

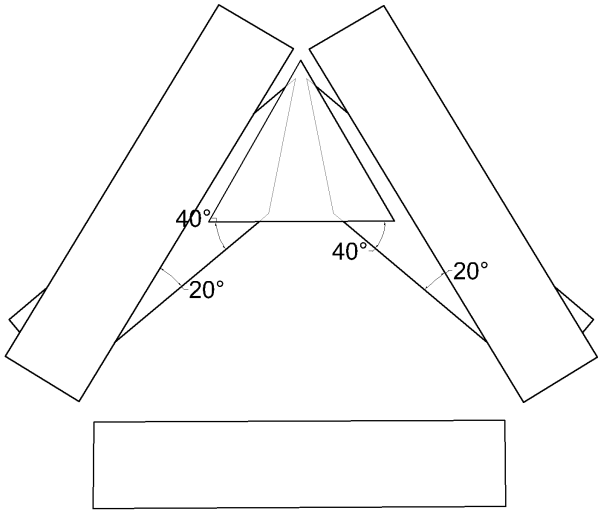

Figure 3.3: An illustration of how a three step bypass is added to the core

4

Methods

To begin with the project a pre-study on power transformers with focus on materials and losses in distribution transformers is done. A literature review in magnetic circuits and measurement techniques for losses and fluxes in the core is also done to have a better understanding of internal dynamics of the working of a power transformers. As the model of core of the transformer is designed by Transformer Cage Core AB, basic information on the working of hexa-core transformer is provided by the company on the flux flow and losses.

With the literature study in place a theoretical model of the core is developed with and without bypass between the different yokes using phasor diagrams. The gap reluctance between the yoke and the bypass pieces are neglected. The phasor diagrams give a better understanding of the flux flows within the core of the transformer.

The setup for measurements is then fixed by adding primary windings in order to magnetize the core. Also search coils to measure fluxes in various points on the transformer are added. The measurements on the core are then done by increasing step wise the voltage across the windings until an approximate theoretical flux density of 2T across one of the legs with intervals of 0.15T. The losses are also measured, by two watt-meter method.

A measurement without bypass is made in order to have a reference. The measurements are then done for all different configurations of single step grain-oriented, two step grain-oriented, three step grain-oriented and single step non-grain oriented for two different areas of cross-section. The changes in the flux magnitude and phase shifts and the core losses are noted. Moreover, between each measurement a new loss reference measurement without bypass is done, in order to not loose the reference loss values.

The measured data for each type of bypass configuration is analyzed for loss reduction, flux magnitude in the bypass and addition of iron in the core. The most optimal solution is derived based on the analysis. Figure 4.1 shows the overall process flow of the project.

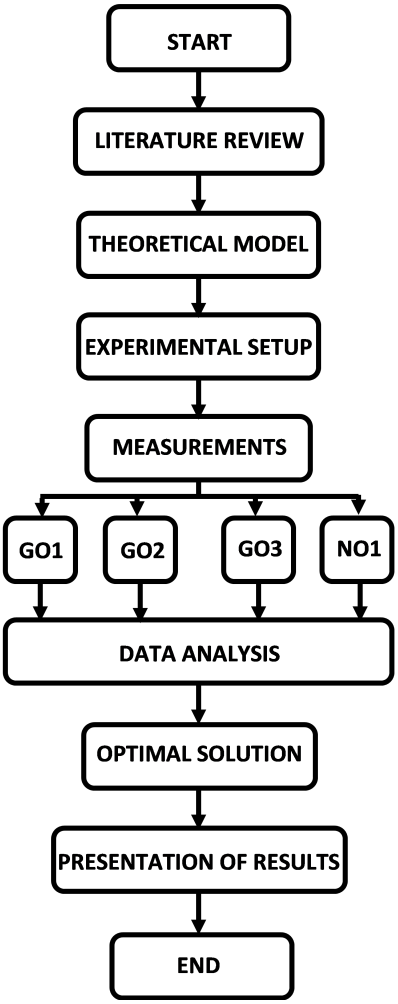

Figure 4.1: General process flow diagram for the project.

5

Measurement equipment and techniques

For the practical analysis of this project a measurement setup is developed. The setup includes a downsized laboratory core wound over by single stranded copper wire. The chapter also focuses on the methods for measuring flux in different sections of the core which includes a search coil and RC integrator circuit. The different measurement points and the instruments used to measure input voltages and currents and also the power dissipated from the circuit are detailed in the latter part of this chapter.

5.1 Transformer core

The transformer core is a downsized laboratory core shown in Figure 5.1. The iron core is constructed from a M4-Oriented Carlite steel. The dimensions and the core type characteristics are shown in Table 5.1. For the other steel specifications provided by the manufacturer see Appendix A.1. The transformer core is developed in such a way that there is approximately $0.5mm$ gap between each layer of the yoke in order to be able to add the bypass pieces to the core.

Figure 5.1: The down-scaled lab prototype of hexa-transformer core.

Specification of Small core		
Specific	Unit	Quantity
Inner width	mm	188
Inner height	mm	340.2
Width of steel	mm	40
Thickness of Steel	mm	0.27
Stacking Factor(Typical)	-	0.97
Area of cross- section of a leg	mm^2	514.56
Volume of core	m^3	7.585e-4
Density of Iron	kg/m^3	7650
Weight of the core	kg	5.803

Table 5.1: Physical specification of the lab core.

5.2 Core windings

The windings on the core are done based on two aspects. First aspect of the coil design being the number of turns which decides the magnitude flux flowing through the core. For a relative high voltage magnitude and feasible number of turns on the core, the number of turns was decided to be 110.

The second aspect is the peak current through the coil when the core is hard saturated. The maximum current at saturation region can be calculated by using the relation between the magneto-motive force and the magnetic field intensity, which can be written as $I = \frac{H\_l}{N}$ where, N is the number of turns,l is the mean flux path which can be calculated using the core dimension data shown in Table5.1, the values of magnetic field (H) at 1.9 T are given by the manufacturer. The calculated maximum current is 10 A at 1.9 T. For selecting the wire to make the coil, the resistive losses from the coil should be neglectable at saturation. Therefore a $3.52mm$ diameter wire winding is used, which can carry according to the standard wire gauge around 52 A. The wire has a resistance of 0.0343Ω, this will give a copper loss below 1% to the total no-load loss in the non saturation region and a maximum of 4% at hard saturation region($\approx 2T$). Since, this value is considerable low compared to the total measured losses the ohmic losses can be neglected.

5.3 No-load loss measurement

Figure 5.2 shows the magnetizing circuit for the transformer core. The setup consists of terminals from a 3 phase, 200V and 50Hz alternator to the core through an auto-transformer and circuit breaker in between. Inputs from the alternator is connected to an 0-470V, 10A, 3 phase auto-transformer to control the excitation voltage of the core within the desired limits. Three ampeters and voltmeters are setup between the auto transformer and the core to measure input currents and phase voltages.

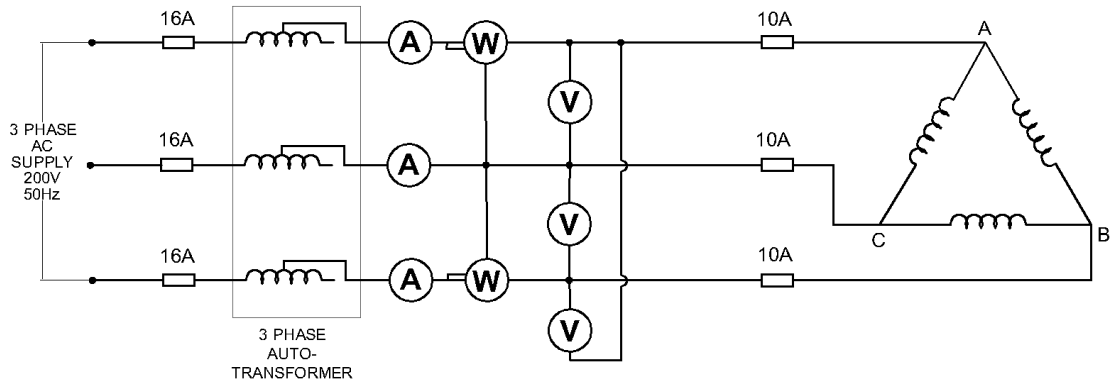

Figure 5.2: Measurement setup.

To measure the total no-load losses in the core, a two watt-meter setup is also added prior to the core windings. Since the measurements done are to analyze the no-load losses in the core, secondary windings are not wound. The inputs are then passed on through 10A fuses to protect the equipment. The primary windings on the core are delta connected.
From theoretical calculations, below a magnetic induction of 1 T in the core the deviation in loss reduction is not significant. Thus the measurements are done between a range of 1 T - 2 T. Table 5.2 shows the different voltage levels required to excite the core to the desired magnetic induction level. The values are calculated by using equation 2.2.

Feeding Voltage [V_{rms}]	Magnetic Induction [T]
12.66	1.00
14.00	1.10
16.00	1.26
18.00	1.42
18.98	1.50
20.00	1.58
21.52	1.70
22.00	1.74
24.00	1.86
25.30	2.00

Table 5.2: Different feeding voltage to excite the core to different magnetic induction level

5.4 Search coil

A search coil is a magnetometer used to measure the flux changes in AC magnetic field. It works using same principles in Faraday's laws of induction. The search coil is basically a loop of wire wound around a magnetic material carrying magnetic flux [13]. Figure 5.3 shows an illustration of the search coil on the section where the flux is to be measured. According to Faraday's law of induction, a time variant magnetic flux passing through a loop of wire induces time variant voltage in it. The induced voltage (V) is proportional to the number of turn and to the negative time rate change of the magnetic flux which can be written as

$$V = -\frac{N\ d\phi}{dt} \tag{5.1}$$

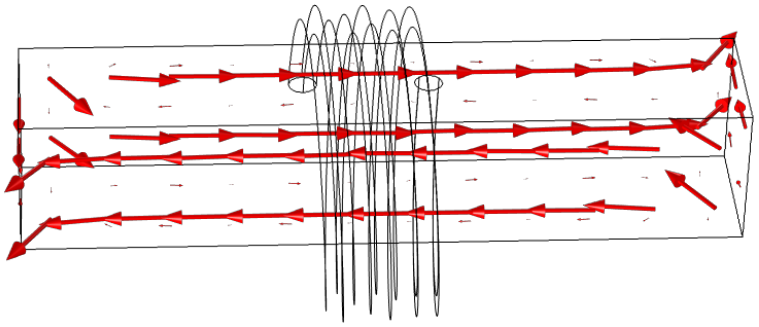

Figure 5.3: Search coil wounded around a ferromagnetic material carrying magnetic flux.

5.5 RC integrator

To measure the flux magnitude in different sections, the output from search coil is fed to an integration circuit. An RC integrator circuit connection is shown in Figure 5.4,where C is series connected with R. The circuit feeding voltage,V_{in} is the induced voltage from the search coil. This circuit is known also as a low pass filter, since it attenuate the high frequencies while it passes through the lower frequencies. A thumb rule for designing such a circuit is to choose the component in a such a way that

$$\omega >> \frac{1}{RC}. \tag{5.2}$$

Where $\omega = 2\pi f$ and f is the frequency. This means that the capacitor will not have enough time to charge up. Moreover, the voltage drop across the capacitor will be very small, therefore V_{in} can be considered to be equal with the voltage across the resistor. This can be shown in the following way. The current i can be written as

$$i = \frac{V_{in}}{Z}, \tag{5.3}$$

where Z is the impedance of the circuit and is equal with

$$Z = R + \frac{1}{j\omega C}. \tag{5.4}$$

From equation 5.2 it follows that $\omega C >> \frac{1}{R}$. This means that the circuit impedance Z can be simplify to $Z \approx R$. Then, equation 5.3 becomes

$$i \approx \frac{V_{in}}{R}, \tag{5.5}$$

which is basically Ohm's law. Now, considering the voltage across the capacitor it follows:

$$V_C = \frac{1}{C}\int_0^t i\ dt. \tag{5.6}$$

Combining 5.3 and 5.6, the following relation can be obtained

$$V_C = \frac{1}{RC}\int_0^t V_{in}. \tag{5.7}$$

Considering the induced voltage, $V_{in} = N\frac{d\phi}{dt}$, the above equation gives that the voltage across the capacitor is equal

$$V_C = \frac{N}{RC}\ \phi. \tag{5.8}$$

This means that the measured voltage across the capacitance gives a good picture about the flux through the search coil.

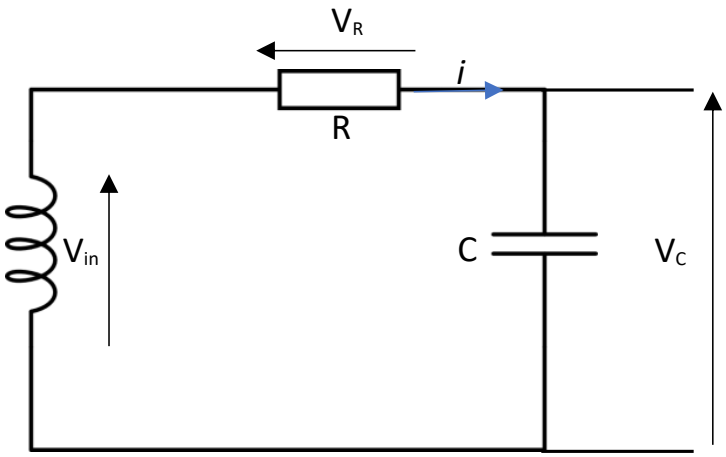

Figure 5.4: An RC integrator circuit in series connection.

Another aspect, which needs to be considered is the introduced phase shift caused by the RC circuit. This can be calculated by using

$$V_{in} = i\ (R - j\frac{1}{\omega C}). \tag{5.9}$$

The component choice for the RC circuit was based on equation 5.2,the ratio $\frac{1}{RC}$ was chosen to be 10. In practice the following components were available to have the ration as close as possible to the chosen value, namely 150 $k\Omega$ resistance and $681nF$ capacitance. This gives a ratio of 9.78 and equation 5.9 becomes

$$V_{in} = i(150\ 10^3 - j4674.2)[V]. \tag{5.10}$$

Assuming, that B=1.7T and a search coil of 10 turns around a core leg with a cross-section area of 518.4 10^{-6} m^2, it will results a voltage $V_{rms} \approx 2V$. Using equation 2.2 and 5.8 result a voltage drop over the capacitance $62mV$ and a phase angle of 1.7°. Since this phase angle is little, it will be neglected.

5.6 Measuring instruments

The tools used to measure different quantities from the experimental setup are shown in Figure 5.5. The instruments are namely,

1. Multi-meters
2. Power-meter
3. Oscilloscope

The specifications of each instrument is detailed in the following subsections.

Figure 5.5: Measuring Instruments used in the project.

5.6.1 Voltmeters and ammeters

To measure the line currents and the phase voltages to the core, six multimeters from FLUKE (FLUKE true RMS 117) are used. The multimeters have a range of 60V and a resolution of 0.01V for the voltage measurements. For current measurements the range is 10A and a resolution of 0.01A. The multi-meters measure the RMS value of the input signal.

5.6.2 Power meter

To measure the power losses in the circuit power meter from Siemens (Siemens Power Meter B4301) is used. It is a two watt-meter setup. The power through the three phases are measured by the power meter with two line currents and the three phase voltages. The power is calculated by finding the average of sum of instantaneous power magnitude over time [12] .

5.6.3 Oscilloscope

To measure the fluxes in different sections of the core, the signal from RC integrator circuit is taken out to an oscilloscope. The oscilloscope used to measure in this project is PicoScope 4824. The oscilloscope has 8 channels with 12-bit resolution and 20MHz bandwidth. The oscilloscope has an accuracy of ±1% of full scale ±300 μV and a range of ±250mV to ±25V.

5.7 Measurement points

The flux in core are measured at specific positions in the core in order to analyze the effect of bypass. Figure 5.6 shows the points at which the search coil is added i

norder to check for the fluxes. These points are namely

1. A_L - Flux in the leg
2. A_1 - Flux in ring between legs A_L and Y
3. A_2 - Flux in ring between legs A_L and X
4. a - Flux in bypass between A_1 and A_2
5. c - Flux in bypass between C_1 and C_2
6. X - Flux at mid-point of yoke between A_L and C_L
7. Y - Flux at mid-point of yoke between A_L and B_L

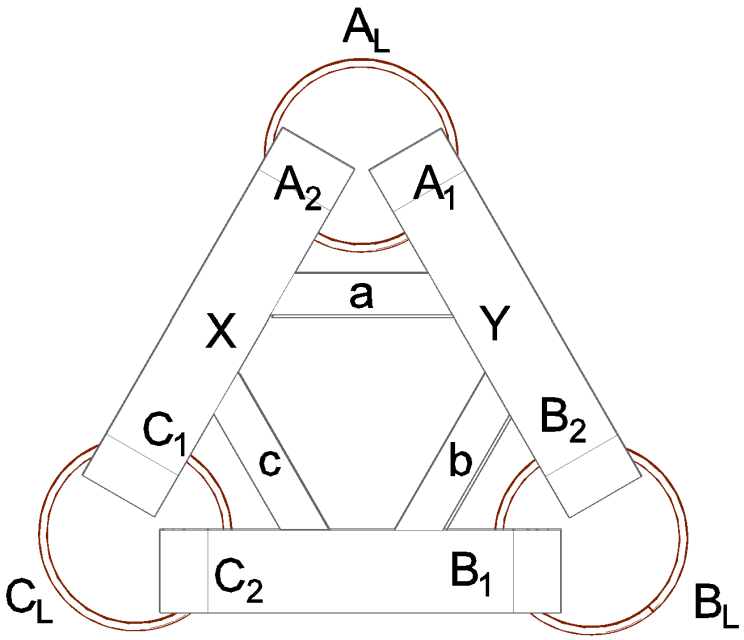

Figure 5.6: An illustration of different sections where flux measurements are done on the core

6

Results

This chapter presents results for the measured values for the different bypass configurations. The results are focused at flux on magnitude and phase shift with respect to flux in leg A of the lab transformer core rings and also the loss reduction.

The results are also focused on the influence of bypass area on the losses and flux magnitude as increase of bypass area potentially influences how much additional iron is added into the core. The presented results are based on two separate area of cross-section for grain-oriented bypass in each configuration and one cross-section area for non-grain oriented configuration.

6.1 Reference measurement

The core without bypass arrangement is setup to measure the flux magnitude on different sections to set a reference point. The losses are also measured to have a comparison between the improvement of having a bypass over the regular laboratory transformer core without a bypass. Figure 6.1 shows the vector diagram for the measured fluxes taken leg A as reference, and normalized to it. The magnitude for ϕ_{B_L} and ϕ_{C_L} are $0.95\phi_{A_L}$ and $1.03\phi_{A_L}$ respectively. Due to the asymmetric nature of the core, the magnitude and phase shift on three legs are different compared to the normalized ideal case.

The deviation from ideal scenario is also reflected in core rings fluxes, with ϕ_{A_1} and ϕ_{A_2} differing in magnitude and phase shifts from leg flux. The phase shift between the leg A and the yoke A_1 and A_2, are α_1=33° and α_2=29°. The flux magnitude relative to the leg, is ϕ_{A_2}=0.51 and ϕ_{A_1}=0.62, respectively. The measured flux magnitude curves in leg A and in the adjoining core rings are shown in Figure 6.2.

Figure 6.3 shows the measured losses in the core over the measured range and the interpolated curve. The interpolated curve is obtained by fitting the measured values with two-term exponential models. As it can be noticed from the figure, the losses in the core increases linearly until 1.6T and beyond this point the losses start increasing exponentially.

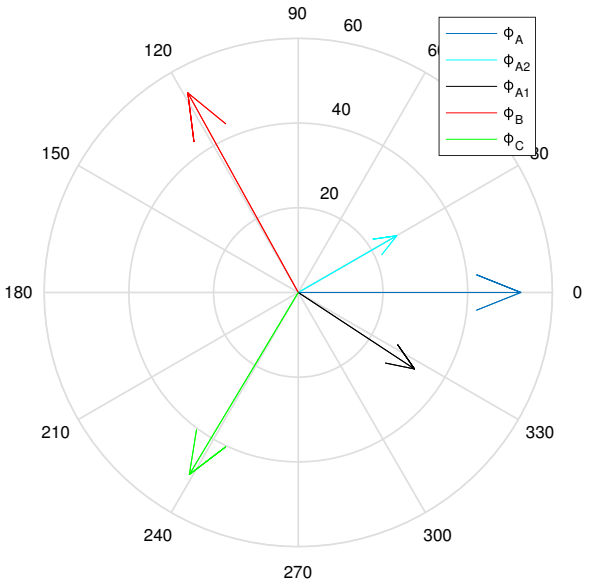

Figure 6.1: Vector diagram for the measured fluxes in legs A,B,C and in yoke ϕ_{A_1} and ϕ_{A_2} at 1.5T without bypass

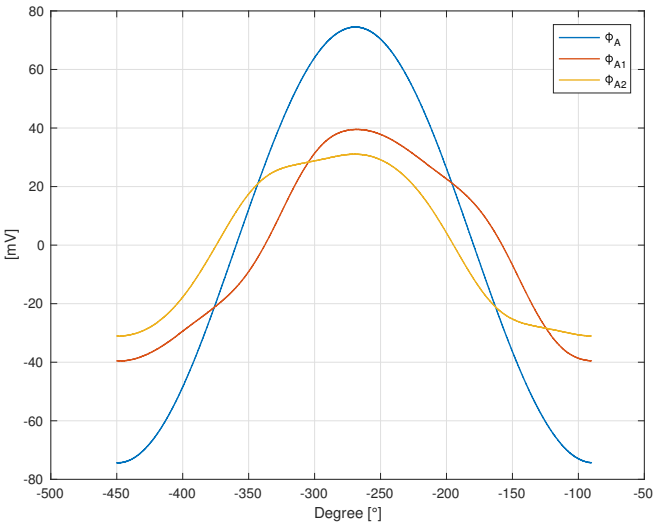

Figure 6.2: Measured fluxes in leg A and the two corresponding core rings at 1.5T without bypass

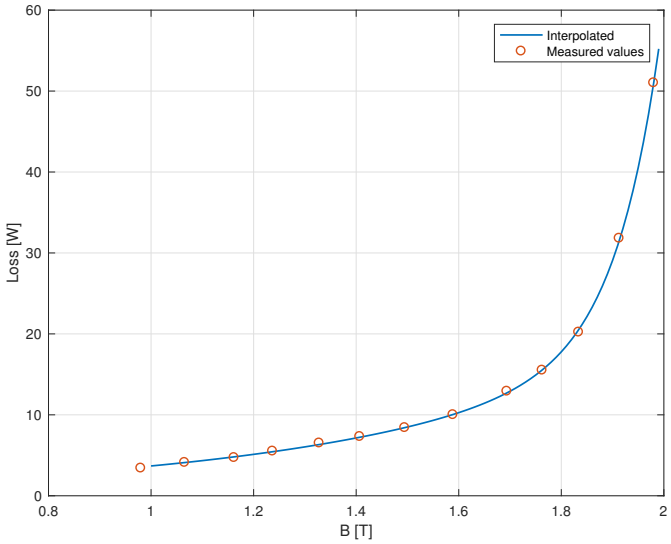

Figure 6.3: The measured losses in hexa-transformer core and the interpolated curve

6.2 One step grain oriented (GO1) bypass

Two different bypass cross sections area were measured, namely $\approx 30\%$ and $\approx 45\%$ of leg area(A_L), to study the flux distribution in the bypass and the resulting loss reduction. This adds on an additional weight to the core rings of 750g and 1125g, respectively. For the bypass configuration with cross section area of $\approx 30\%$ a bypass unit was placed in between every slot with a total of five slots for each bypass units,

to have an evenly distributed bypass through the yoke area. Moreover, the bypass from the other yokes was placed on different slot, to avoid flux collision in the yoke. On the other hand, bypass cross section area of 45% was achieved by placing two bypass pieces in five slot and five single bypass pieces in the remaining slots. In this case the yoke which contains the less slots was fully bypassed. Figure 6.4 and 6.5 shows the measured values, the resulting interpolated curve based on the measured values in case of 30% and 45% of leg cross section area and the reference interpolated curve for comparison. The interpolation is done with the same model as the reference loss curve, i.e. two-term exponential model.

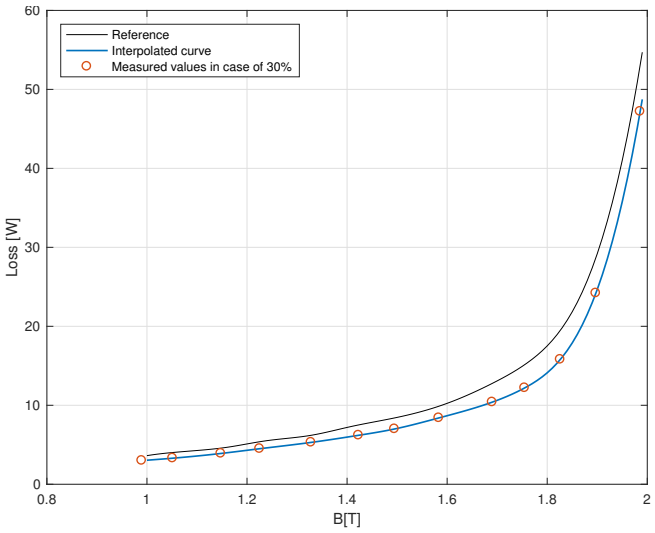

Figure 6.4: The reference curve and the interpolated loss curve based on the measured values in case of 30% GO1 bypass cross section area

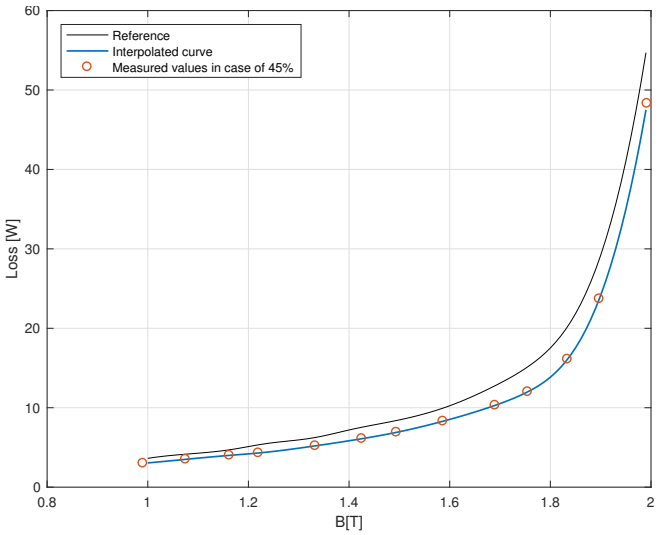

Figure 6.5: The reference curve and the interpolated loss curve based on the measured values in case of 45% GO1 bypass cross section area

Figure 6.6 shows the difference in percentage from the reference loss curve for the two cross section areas. The differences are obtained from the interpolated curves. As it can be observed from the figure,the loss reduction varies between ≈ 15% and ≈19.5% in case of 45% of leg cross section area and for 30% varies between ≈ 14.7% and ≈18%. Figure 6.7 shows the measured flux curves in leg A,the adjoining core

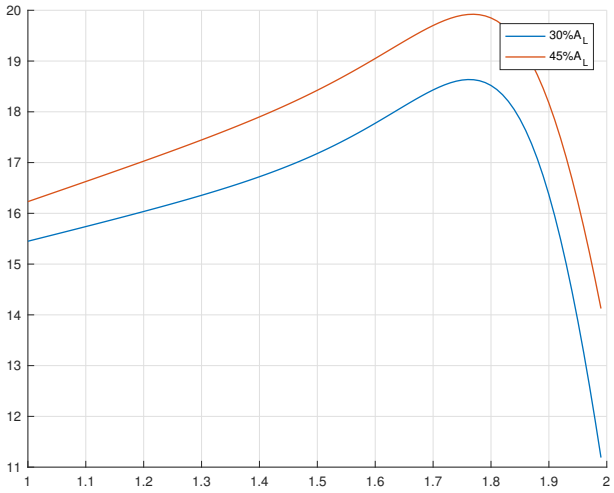

Figure 6.6: Loss reduction in case of 30% and 45% GO1 bypass cross-section area compared with the reference curve

rings fluxes A_1, A_2 and the flux in the bypass for the two different bypass cross section area wave shapes at 1.5T.

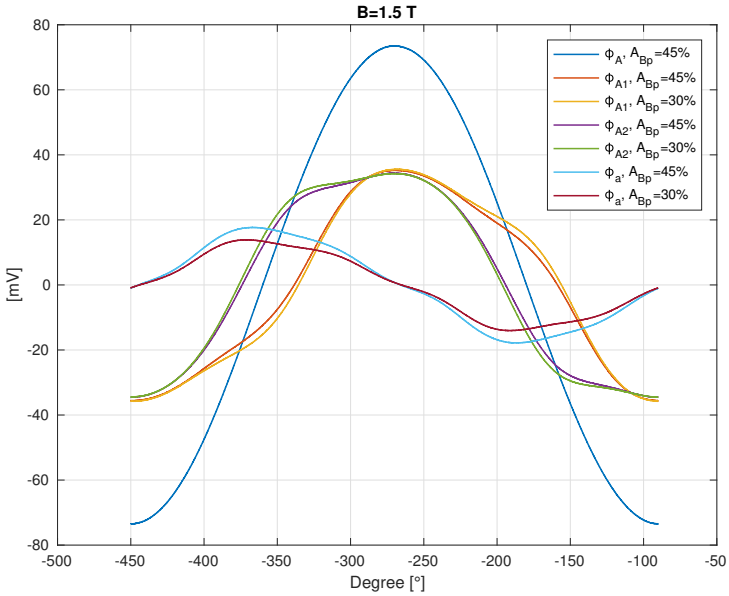

Figure 6.7: Measured fluxes in leg A for two different cross section area at 1.5T

Table 6.1 shows the flux values normalized to the flux in the leg for different fluxes at 1.7T and 1.5T for the two different cross section area. The ratios are obtained by using the *rms* values of the measured magnetic flux curves. As it can be seen, different magnetic induction gives different flux ratios.

B[T]	ϕ_{A_1}/ϕ_{A_L}	ϕ_{A_2}/ϕ_{A_L}	ϕ_a/ϕ_{A_L}	ϕ_c/ϕ_{A_L}	$\alpha_1[°]$	$\alpha_2[°]$	ϕ_X/ϕ_{A_L}	ϕ_Y/ϕ_{A_L}
Bypass cross section area 30% of the leg								
1.5	0.49	0.514	0.1797	0.14	24.2	16.5	0.5889	0.581
1.7	0.485	0.51	0.185	0.148	23.8	16.8	0.5755	0.5927
Bypass cross section area 45% of the leg								
1.5	0.48	0.505	0.227	0.171	21.45	14.07	0.6016	0.5886
1.7	0.4774	0.502	0.23	0.177	21.43	14.42	0.6022	0.5898

Table 6.1: Measured values for flux and phase shifts normalized to leg A_L for GO1 bypass configuration

Figure 6.8 shows the vector diagram for the measured fluxes with a cross-section area of bypass at 30% and Figure 6.9 shows the vector diagram of the measured magnetic flux for 45% cross-section area,respectively. The phase angle at point Y and X are 35.6° and 29.6° with a cross section area of 30% in contrast to 37° and 30.8° with a cross section area of 45%.

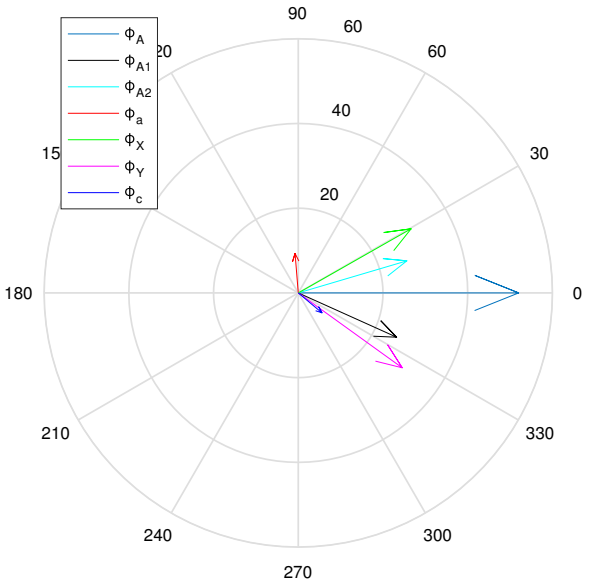

Figure 6.8: Vector diagram at 1.5T for the measured flux in leg A with a cross section area 30%.

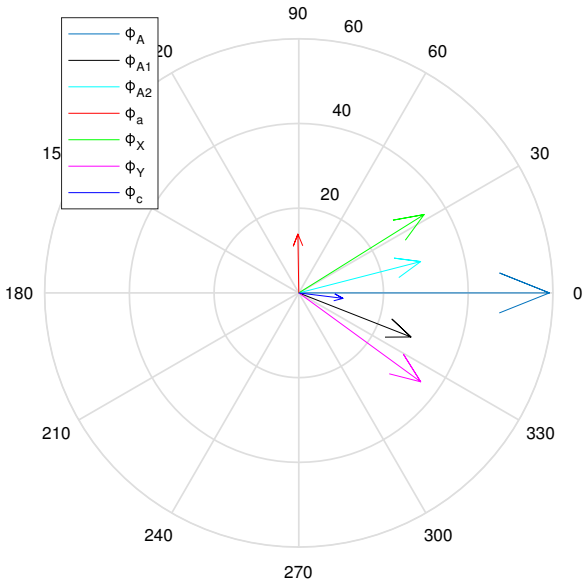

Figure 6.9: Vector diagram at 1.5T for leg A with a cross section area 45%.

6.3 Two step grain oriented (GO2) bypass

Two bypass cross section area are measured for this type of configuration, namely ≈ 22% and ≈ 32% of the leg cross-section area. This adds on an additional weight of

1310g and 1965g, respectively. Figure 6.10 and 6.11 show the interpolated loss curve and the measured values for the two different cross section area with the reference interpolated loss curve for comparison.

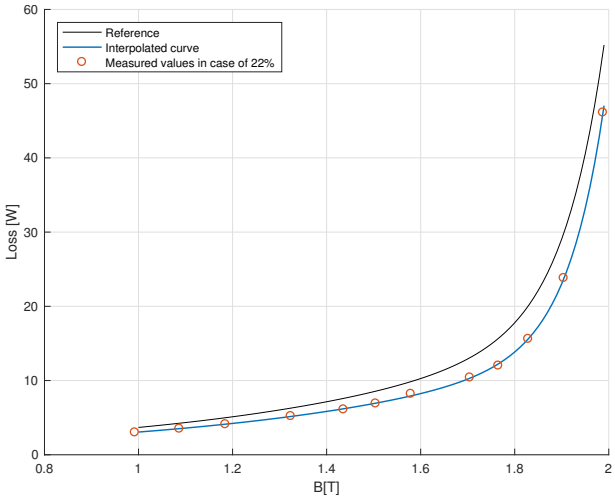

Figure 6.10: The reference curve and the interpolated loss curve based on the measured values in case of 22% GO2 bypass cross section area

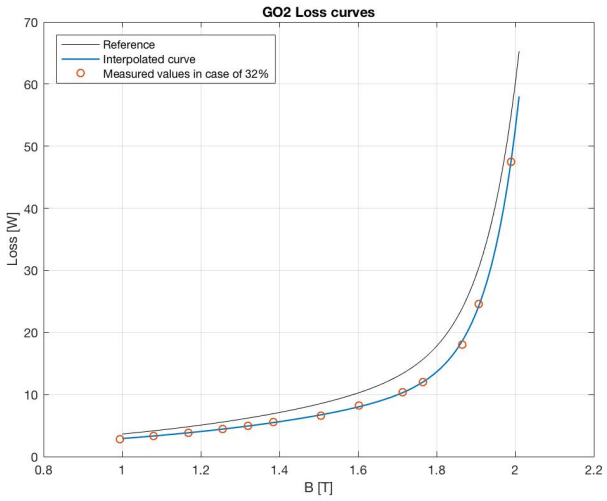

Figure 6.11: The reference curve and the interpolated loss curve based on the measured values for 32% GO2 bypass cross section area.

Furthermore, Figure 6.12 shows the difference in percentage from the reference loss curve for both cross-section area. The differences are obtained from the interpolated curves.

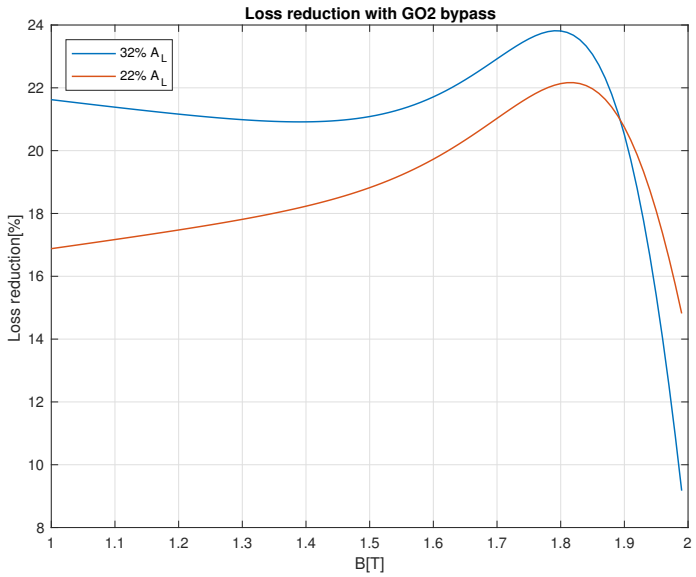

Figure 6.12: GO2 loss reduction from the reference for two different cross section area.

As it can be observed, the loss reduction in case of a bypass cross section area of 22% of the leg cross section area(A_L) varies between 16% and 22% and for a cross section area of 32%A_L varies between 20% and 23.5%. The obtained flux curves are shown

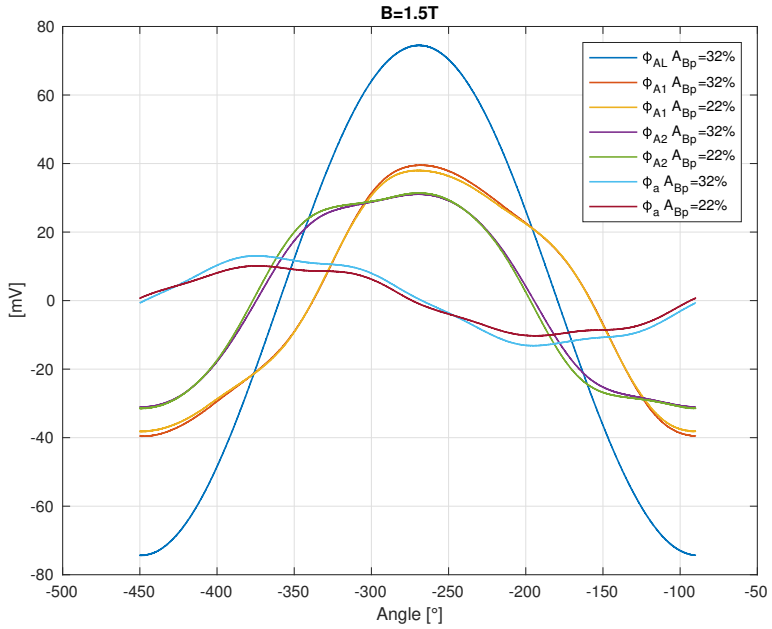

Figure 6.13: Flux in the yoke and the bypass for two different cross section area at 1.5T.

in Figure 6.13 for the two different cross sections. Table 6.2 shows different flux values relative to the leg flux. It also details on the phase angles of both α_1 and α_2. Figure 6.14 and Figure 6.15 shows the vector diagrams for both the cross-sections using GO2 bypass configuration. The phase angle at point X and Y are 29° and 34°, respectively for a bypass cross section area of 32%A_L, and 29° and 30° for a bypass cross section area of 22%A_L.

Bypass cross section area 22% of the leg								
B[T]	ϕ_{A_1}/ϕ_{A_L}	ϕ_{A_2}/ϕ_{A_L}	ϕ_a/ϕ_{A_L}	ϕ_c/ϕ_{A_L}	$\alpha_1[°]$	$\alpha_2[°]$	ϕ_X/ϕ_{A_L}	ϕ_Y/ϕ_{A_L}
1.5	0.5274	0.4683	0.155	0.15	21.1	17.6	0.5889	0.581
1.7	0.52	0.467	0.158	0.155	21	17.8	0.5163	0.6121
Bypass cross section area 32% of the leg								
1.5	0.535	0.4519	0.1758	0.1639	21.7	15	0.56	0.57
1.7	0.5324	0.4474	0.184	0.174	21.1	15.2	0.55	0.582

Table 6.2: Significant measurement values for flux and phase shifts normalized to leg A_L for GO2 bypass configuration.

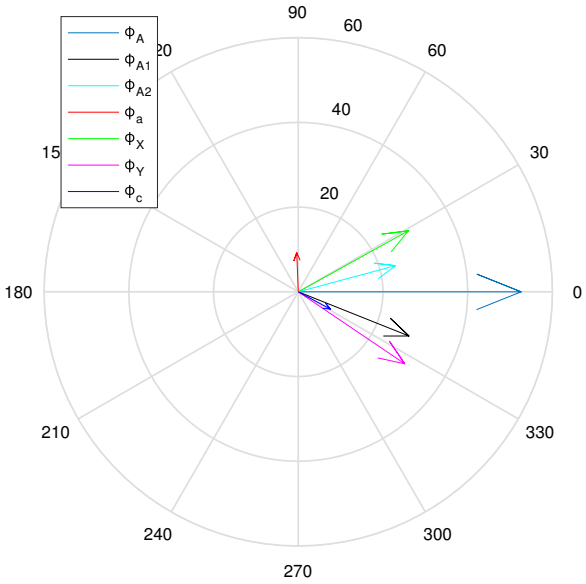

Figure 6.14: Vector diagram for GO2 bypass with 32% cross-section area.

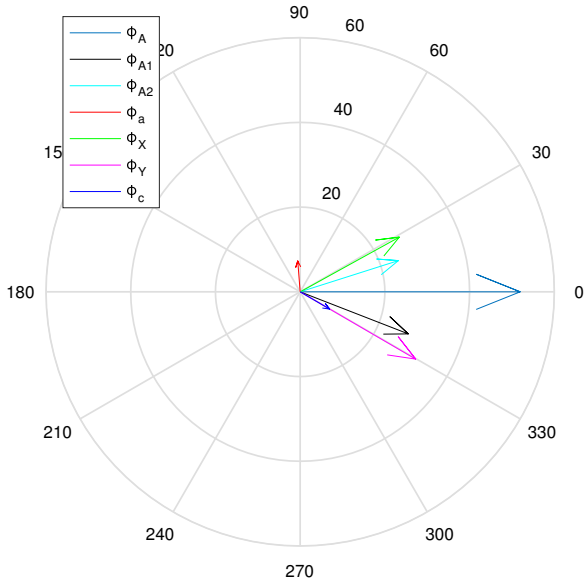

Figure 6.15: Vector diagram GO2 bypass with 22% cross-section area.

6.4 Three step grain oriented (GO3) bypass

Three step grain oriented bypass (GO3), similar to GO2 bypass is measured for two separate area of cross-sections. These have a cross section area of $\approx 30\%$ and $\approx 53\%$ of the leg area, respectively. For the 30% the bypass is configured to the ten slots setup with one layer of yoke between each layer from the inner half of the yoke and utilizing a total of 5 slots for each bypass unit. The bypass cross section area of 53% A_L is achieved by increasing the number of bypass slots of the previous cross section to nine slots.For each of 30% and 53% type the total steel added to the core are 1362g and 2450g, respectively.
The measured losses and the interpolated curves for each cross section area with the reference interpolated loss curve presented in Figure 6.16 and 6.17, respectively. The total loss reduction made by this configuration is shown in Figure 6.18 in percentage. As in the previous configurations the reduction plot is obtained by taking the difference between the interpolated curves.

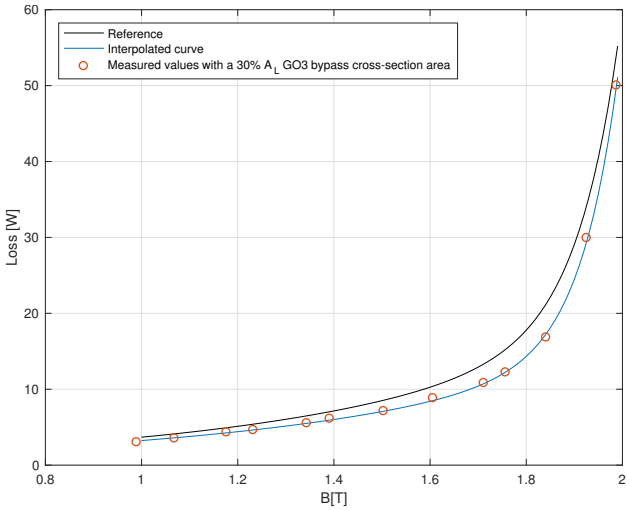

Figure 6.16: Interpolated loss curve for measured values in case of 30% cross section area and the reference loss curve

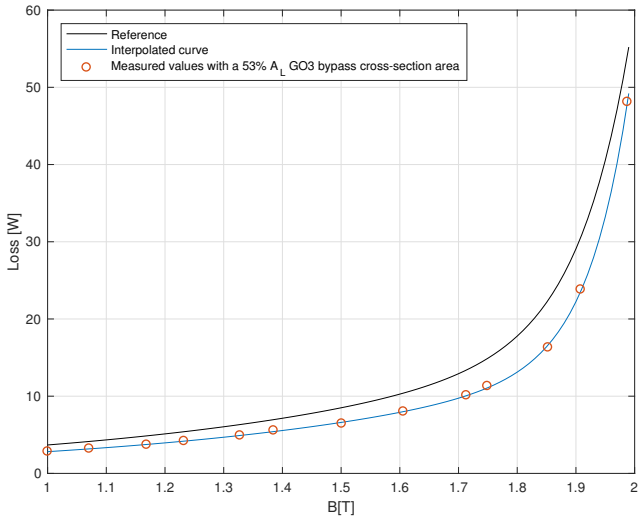

Figure 6.17: Interpolated loss curve for measured values in case of 53% cross section area and the reference loss curve

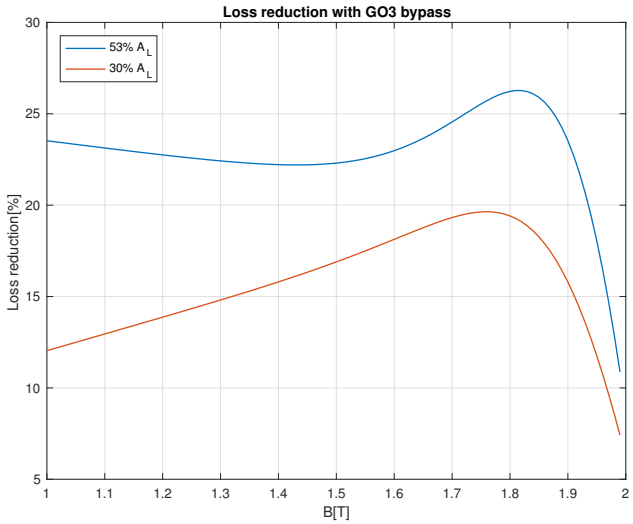

Figure 6.18: Loss reduction for two different cross section area for GO3 bypass

The measured values of loss reduction between 1T-1.8T varies between 22.5% to 26.5% for 53% of cross-section area and 12.5% to 20% for 30% of cross-section area. The measured flux curves in leg A_L, in the adjoining core rings A_1, A_2 and in the bypass, for both the configurations at 1.5T are shown in Figure 6.19. Table 6.3 shows the different flux ratios relative to the flux in leg A and the phase shift from the adjoining core rings α_1 and α_2.

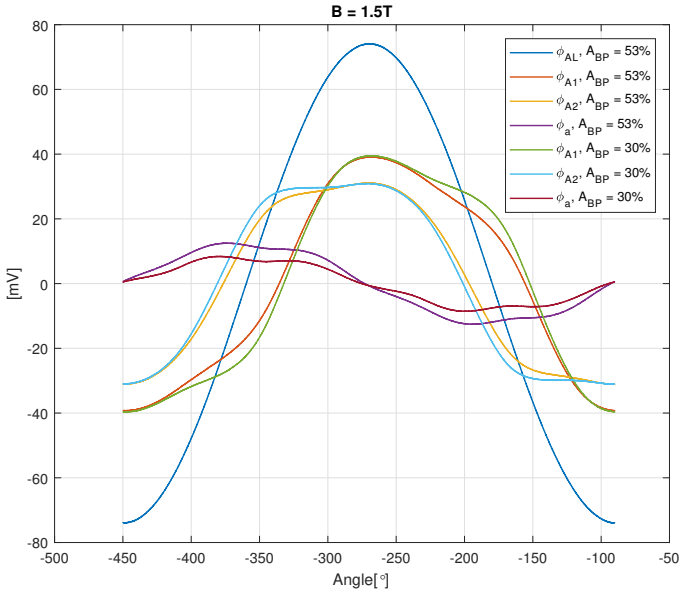

Figure 6.19: Measured fluxes in different sections in GO3 bypass 1.5T

Bypass cross section area 30% of the leg								
B[T]	ϕ_{A_1}/ϕ_{A_L}	ϕ_{A_2}/ϕ_{A_L}	ϕ_a/ϕ_{A_L}	ϕ_c/ϕ_{A_L}	$\alpha_1[°]$	$\alpha_2[°]$	ϕ_X/ϕ_{A_L}	ϕ_Y/ϕ_{A_L}
1.5	0.5595	0.4770	0.1102	0.0870	27.63	21.03	0.5685	0.5866
1.7	0.5579	0.4683	0.1224	0.0992	26.10	21.13	0.5605	0.5913
Bypass cross section area 53% of the leg								
1.5	0.5386	0.4617	0.1683	0.1370	24.17	16.84	0.5724	0.5875
1.7	0.5355	0.4556	0.1799	0.1495	22.95	16.55	0.5654	0.5902

Table 6.3: Significant measurement values for flux and phase shifts normalized to leg A_L for GO2 bypass configuration.

Figure 6.20 shows the measured fluxes' magnitude and phase in a phasor diagram in case of a cross section area of 30 % of leg area and Figure 6.21 shows the vector diagram for a bypass cross section area of 53% A_L. The phase angles for measurement points X and Y are 29°and 34.6°respectively for configuration with a bypass cross section area of 30% A_L. Furthermore, for the bypass cross section area of 53% of A_L configuration, angles are 29.3°and 35.4°, respectively.

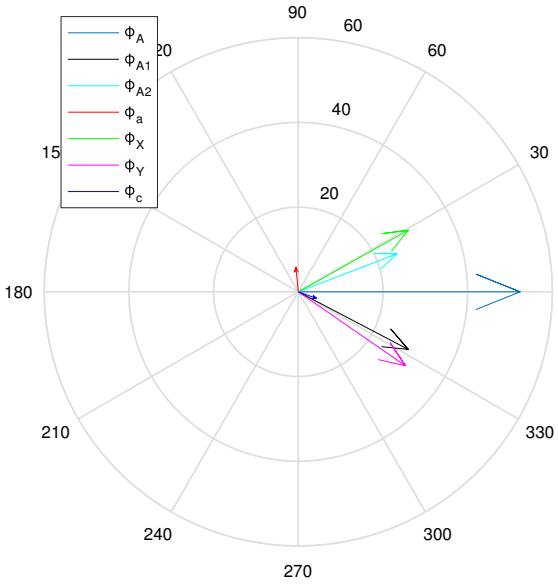

Figure 6.20: Vector diagram GO3 bypass with 30% cross-section area.

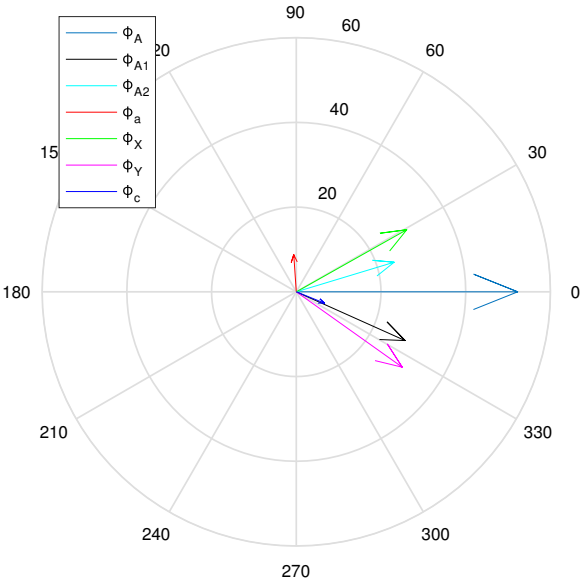

Figure 6.21: Vector diagram GO3 bypass with 53% cross-section area.

6.5 One step non-grain oriented (NO1) bypass

The non-grain oriented steel bypass (NO1) configuration was measured with one piece of bypass piece per slot. The bypass was setup with five equally spaced slots in the yoke with one slot between two layers of yoke. The bypass cross-section area measured to approximately 14% of the leg area(A_L). The total weight of steel added to the core for addition this bypass is 484g. Figure 6.22 shows the measured losses for core over a range of 1T to 2T. Figure 6.23 shows the loss reduction with a NO1 bypass. The range of values change from ≈8% at 1T to 2.9% at 1.5T and then increases to ≈ 13% at 1.85T.

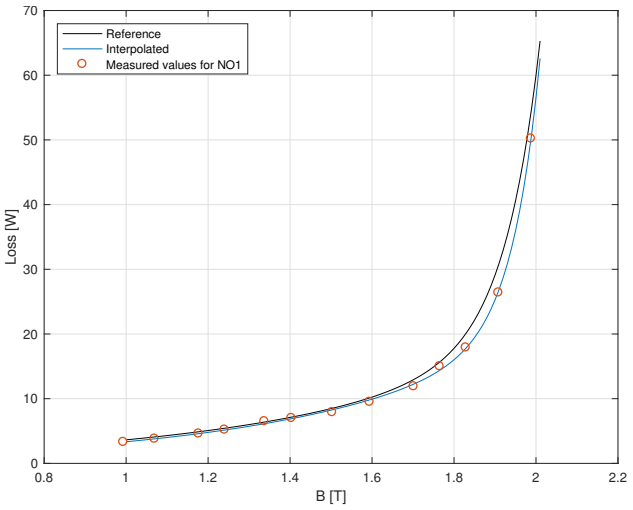

Figure 6.22: Interpolated loss curve for NO1 bypass based on the measured values and the reference loss curve for comparison.

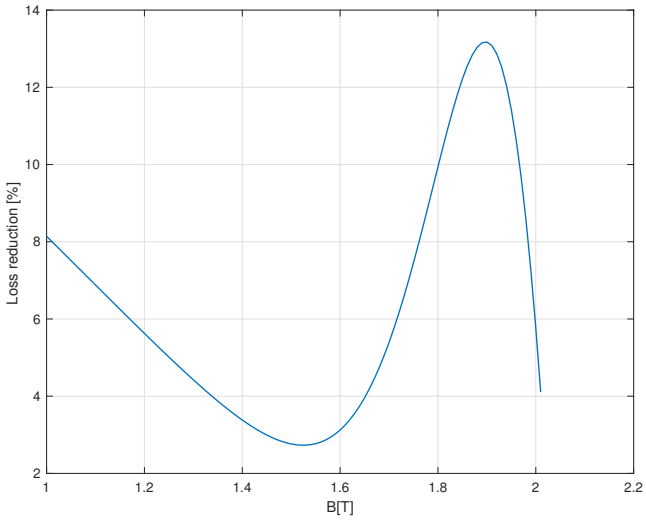

Figure 6.23: Loss reduction with NO1 bypass.

The flux in different sections of core, which include flux in the leg A_L, flux in adjoining yokes A_1 and A_2 and the flux in in bypass are shown in Figure 6.24. From the obtained flux curves, magnitudes of fluxes in yoke and bypass normalized with flux in leg and phase shifts are calculated. Table 6.4 shows a detailed chart of flux data of core mentioned sections of the core at 1.5T and 1.7T.

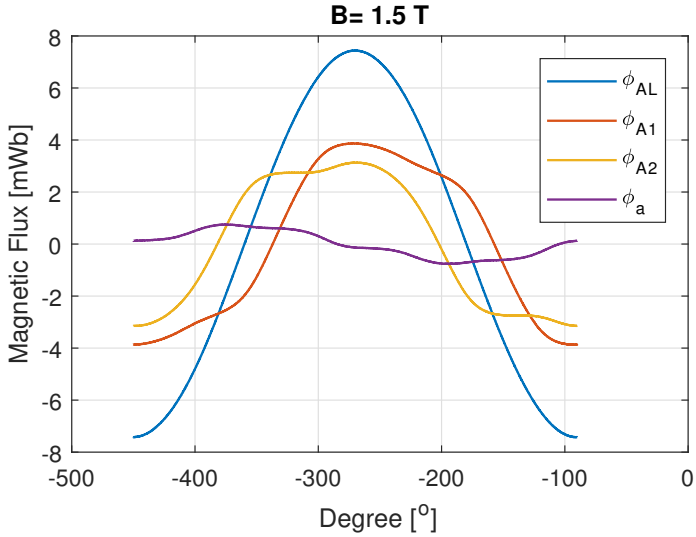

Figure 6.24: Measured fluxes in different sections in NO1 bypass.

B[T]	ϕ_{A_1}/ϕ_{A_L}	ϕ_{A_2}/ϕ_{A_L}	ϕ_a/ϕ_{A_L}	ϕ_c/ϕ_{A_L}	$\alpha_1[^\circ]$	$\alpha_2[^\circ]$	ϕ_X/ϕ_{A_L}	ϕ_Y/ϕ_{A_L}
1.5	0.552	0.4676	0.0938	0.1405	22.91	21.98	0.4947	0.6190
1.7	0.538	0.4631	0.1144	0.1516	21.67	20.88	0.4975	0.6091

Table 6.4: Significant measurement values for flux and phase shifts normalized to leg A_L for NO1 bypass configuration.

The vector diagrams for significant fluxes associating to leg A are shown in Figure 6.25 for 1.5T. The phase angles at X and Y are 29°and 28.5°respectively.

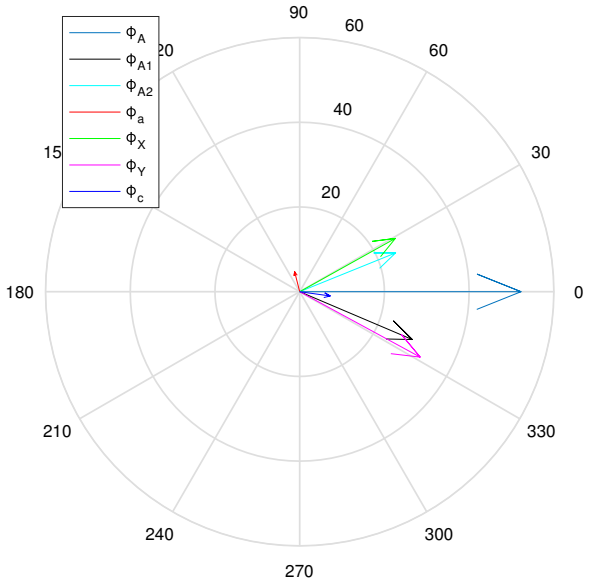

Figure 6.25: Vector diagram for the measured flux at 1.5T for NO1

7

Analysis

The introduction of magnetic bypass in the core reduces the no-load losses. The improvements are subdivided as loss improvement from each of different types of bypass and reduction of flux magnitude in yokes are analyzed in this chapter. Furthermore, how increase of area of cross-section of bypass affects loss reduction and flux in the bypass are also analyzed in latter part of this chapter. Finally, an optimal solution to the problem, based on how much steel is added and how much improvement is derived.

7.1 Alpha and flux magnitude analysis based on type of bypass

According to the theory, α_1 and α_2 are controlled by the flux magnitude in the bypass. Since, the system is unbalanced, the flux magnitude in the bypasses are different. Figure 7.1 and 7.2 shows the measured flux ϕ_a and ϕ_c for the different bypass cross-section area and configurations. It can be noticed that in case of GO1 the measured flux magnitude ϕ_a at around 30% cross-section area shows the highest flux magnitude followed by GO2 and in case of a cross-section area of 45% of A_L GO1 has the highest flux magnitude. Although, in case of GO2 the flux in the bypasses shows the most balanced distributions. It can also be noted that the flux magnitude through NO1 bypass is the least. The cross-section area of NO1 bypass is much smaller (14% of leg area) compared to the grain-oriented bypass configurations. Along with the higher losses from the material, cross-sectional area also plays an important role in pushing the results down for a non-grain oriented bypass. Therefore, making it hard to reach a conclusion for NO1 bypass.

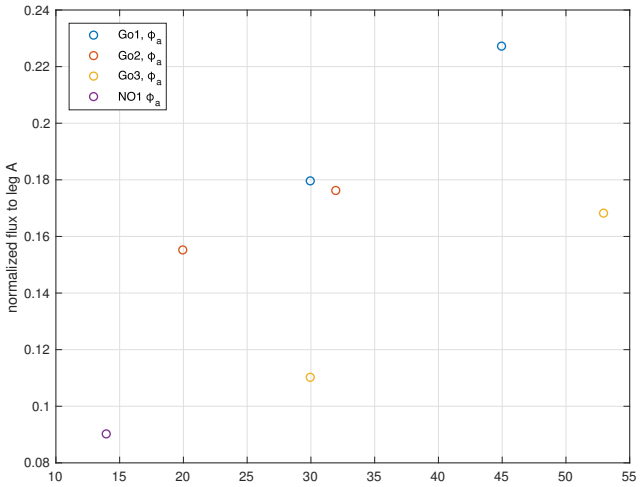

Figure 7.1: Flux ϕ_a in different bypass configurations and cross-sections.

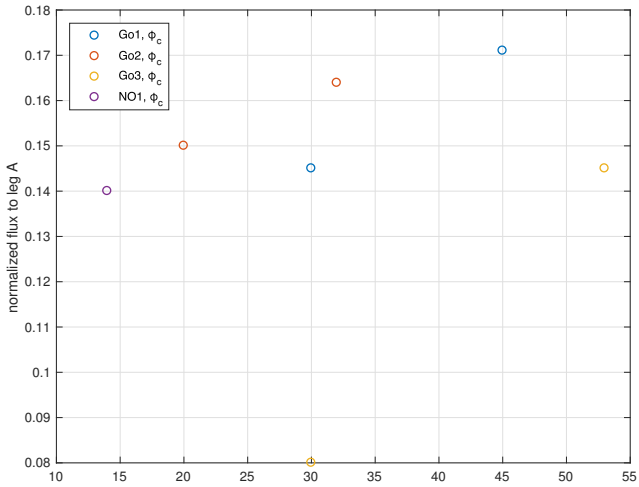

Figure 7.2: Flux ϕ_c in different bypass cross-section area.

Figure 7.3 shows the measured α_2 for the different configurations and the theoretical α_2 reduction based on the flux magnitude ϕ_a in the bypass. It can be seen that the theoretical curve and the measured α_2 doesn't fit. Since, in the theoretical calculation the flux vectors are assumed to be symmetrical the deviations are understandable. Moreover, as we could see in the result chapter, the increase in bypass cross-section area drove X and Y point away 30° phase shift from the flux in the leg, instead of decreasing α. This happened due to fact that the difference between the flux magnitude in the bypasses($|\phi_a|, |\phi_c|$) increased as the bypass cross-section area increased. As a consequence, the phase shift between the bypasses are decreased (>120°) with increased bypass cross-section area. Since the system from the beginning is unbalanced, and the core mechanical condition is unknown, it is hard to point out the main reason for this phenomena.

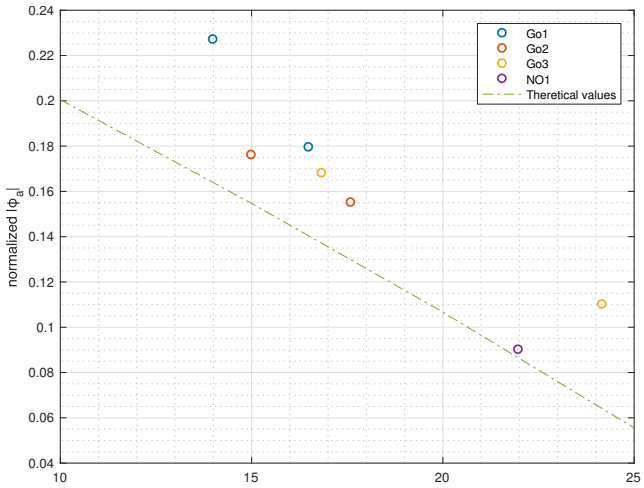

Figure 7.3: Measured flux magnitude and the corresponding angle α_2 compared with the theoretical calculated value.

7.2 Loss analysis

Figure 7.4 shows how much loss is reduced in each type of bypass with different cross-section area and in Figure 7.5 shows the theoretical loss reduction curves. It can be noticed that the measured loss reduction curve matches the theoretical loss reduction curve, between a range from 1T to 1.3T. However, the peak values are less than in the theoretical values, which is expected due to several reasons,

- in the theoretical calculation the loss in the bypass is not considered
- the core is assumed to be symmetric,which is not in this case
- there are possibility that the lamination in the slots are violated
- the voltage reading at saturation region jumping between several voltage level, therefore the reading is taken the average between the maximum and the minimum reading value

As a consequence, a full comparison cannot be made, as well to draw a conclusion about the theoretical calculation based on the measured loss curves above 1.4T.

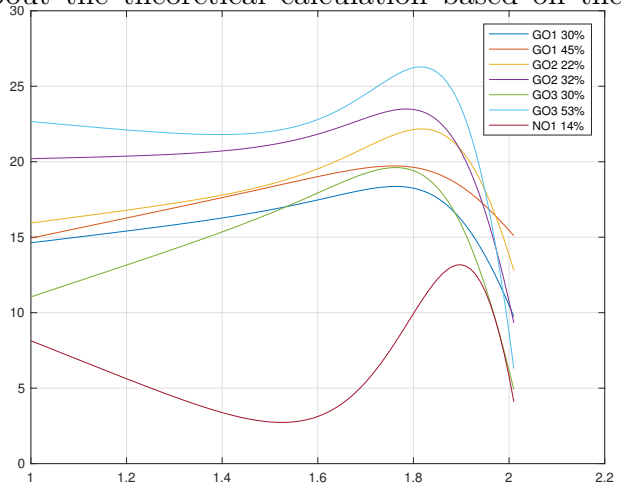

Figure 7.4: Loss reduction in all the different bypass configurations.

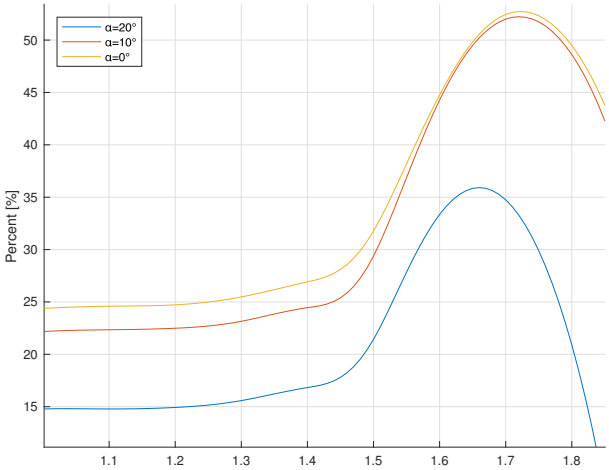

Figure 7.5: Theoretical reduction curves for different angle α.

Moreover, it can be noticed, that the loss reduction is the highest in case of GO3 with a cross-section area of 53% of leg cross-section area (A_L), followed by GO2. As in the previous sub-chapter could be noticed, in case of GO2 the difference between the magnitude of bypass fluxes (ϕ_a, ϕ_c) showed the most balanced compared with GO1 bypass. Furthermore, it can be seen that the flux magnitude in the bypass has an effect on the loss curve as the angle α reduces. This means that the theoretical approach with the α reduction holds.

7.3 Optimal solution

The ferromagnetic materials and the copper are finite resources. As the technological development in the power system progresses in direction to reduce CO_2 emissions and make the system as sustainable as possible, a consequence can be that the usage of these natural resources will be increased and it can diminish in the future. Therefore, it is necessary to take into account the amount of natural resource usage

behind every technological innovation.

The bypass method will require additional iron to be added to the transformer core, however this will not lead to an increase of core leg cross-section area.
Hence, the most optimal solution is derived based on how much loss reduction is achieved in the core, the complexity of the bypass and the weight of the iron added to the core. Table 7.1 shows the significant quantities for the analysis of optimal bypass configuration. From the data it can be seen that GO3 configuration with a bypass area of 53% has the best lost reduction at 1.5T. But the total weight of iron added to the core is approximately 2.5kg. GO1 configuration with 45% of bypass cross-section, has highest flux magnitude in bypass and least addition of iron weight.

Type of Bypass	Area of cross-section to leg area [%]	Weight of iron added [g]	Flux magnitude in bypass [p.u]	Loss Reduction [%]
GO1	30	750	0.18	≈14.7 - ≈18.0
GO1	45	1125	0.23	≈15.0 - ≈19.5
GO2	22	1310	0.15	≈16.0 - ≈21.5
GO2	32	1965	0.18	≈20.0 - ≈23.5
GO3	30	1362	0.11	≈12.5 - ≈20.0
GO3	53	2450	0.17	≈22.5 - ≈26.5
NO1	14	484	0.09	≈2.9 - ≈13.3

Table 7.1: Comparison of all significant quantities in measurement.

8

Conclusion

This study analyzes the effect of magnetic bypass on no-load losses in a down scaled hexa-transformer core. Due to a manufacturer defect, the core is unbalanced between the phases. Four different bypass configurations were analyzed, GO1, GO2, GO3 and NO1 in order to determine the optimal solution.

In the theoretical calculation it was showed that the introduced bypass in the transformer core decreases the magnetic flux magnitude in the core rings and phase angle α, between the core ring and the leg. Moreover, it was showed that the loss reduction is a function of phase angle α, which is controlled by the magnetic flux magnitude in the bypass .

From the result, it could be observed that the increased magnetic flux in the bypass decreased the flux magnitude in the core ring by reducing the phase angle,α. Consequently, the decreased phase angle α reduced the no-load loss in the transformer. However, a comparison between the theoretical calculation and the measured values cannot be made, due to the fact that in the theory the core is assumed to be symmetric, but the measurement is done on an unbalanced core. Although, the theoretical loss reduction calculation gave a good match with measured values at low magnetic induction level. The highest loss reduction of $\approx 22.5\%$ to $\approx 26.5\%$ was achieved in GO3 type of bypass for different induction levels, with an additional of 40% of the total core weight added to the core and a magnetic flux of 0.17 p.u.

In addition, the highest magnetic flux magnitude through the bypass was measured in GO1 type of bypass. Therefore, it is believed, that in case of a symmetric core, this type of bypass will perform a higher no-load loss reduction than GO2 type of bypass. Moreover, in a sustainable perspective, this type of bypass requires the less added iron to the core, which makes this bypass the most optimal between the other bypasses.

It is important to stress, that for NO1 bypass, the measured cross-section area is the least between the other type of bypass cross-section areas. Moreover, the steel material has a high rated loss, therefore a conclusion cannot be made.

Bibliography

[1] European Environment Agency (EEA), "Overview of electricity production and use in Europe",2016. [Online]. Available: https://www.eea.europa.eu/data-and-maps/indicators/overview-of-the-electricity-production-2/assessment, Accessed on:06-04-2018

[2] Wolfgang Irrek, Frangiskos Topalis, Roman Targosz, Anne Rialhe, Juan Frau, 'Policies and Measures Fostering Energy-Efficient Distribution Transformers', SEEDT, Project No. EIE/05/056/SI2.419632. [Online]. Available at: www.seedt.ntua.gr/.

[3] COMMISSION REGULATION (EU) No 548/2014 of 21 May 2014 on implementing Directive 2009/125/EC of the European Parliament and of the Council with regard to small, medium and large power transformers, 2009. [Online]. Available at: https://publications.europa.eu/en/publication-detail/-/publication/9124a197-e17f-11e3-8cd4-01aa75ed71a1/language-en, Accessed on: 02-02-2018

[4] Alex Goldman, 'The Handbook of Modern Ferromagnetic Materials', New York: Springer Science+Business Media, 1999 [Online]. Available at: https://www.springer.com/gp/book/9780412146619, Accessed on: 04-06-2018

[5] Robert M. Del Vecchio; Bertrand Poulin; Pierre T. Feghali; Dilipkumar M. Shah; Rajendra Ahuja, 'Transformer Design Principles: With Applications to Core-Form Power Transformers', Second Edition, CRC Press, June 2010

[6] B. H. E. Limited, BHEL and AccessEngineering (e-book collection), transformers. (2nd ed.) 2003.

[7] W.W. Lewis, "LOSSES IN A TRANSFORMER" presented at Midwinter Convention of the American Institute of Electrical Engineers, New York, 1913, pp 477-509, [Online]. Available : https://ieeexplore.ieee.org/document/6661191/, Accessed on :24-04-2018

[8] M. A. Bahmani, E. Agheb, T. Thiringer, H. K. Høidalen, and Y. Serdyuk, 'Core loss behavior in high frequency high power transformers—I: Effect of core topology', Journal of Renewable and Sustainable Energy, vol. 4, no. 3, 2012, [Online]. Available : https://doi.org/10.1063/1.4727910, Accessed on: 24-04-2018

[9] S. Lundmark and Y. V. Serdyuk and S. M. Gubanski and B. Larking, 'Comparison between hexa- and conventional E-type core three-phase transformers', 2008 18th International Conference on Electrical Machines, 2008 [Online]. Available at: https://ieeexplore.ieee.org/document/4799835/, Accessed on: 24-04-2018

[10] NORDTRAFO, 3-Fas Hexatransformator 5-50 kVA IP00-Nordtrafo' 2018. [Online]. Available at: https://www.nordtrafo.se/transformatorer/produkt/3-fas-hexatransformator-5-50-kva-ip00/, Accessed on: 05-05-2018
[Online] Available:http://m.energy.siemens.com, Accessed 05-05-2018

[11] Yuki MORI, Daisuke MIYAGI, Masanori NAKANO, Norio TAKAHASHI, 'Measurement of Magnetic Properties of Grain-Oriented Electrical Steel Sheet Using 2D Single Sheet Tester' [Online] Available:http://pe.org.pl/articles/2011/9b/10.pdf, Accessed 06-03-2018

[12] Martin U. Reissland, 'Electrical Measurements: Fundamentals, Concepts, Applications', Wiley,1989.

[13] Schubert, Gerald. (2015). Treatise on Geophysics, 11 Volume Set (2nd Edition) - 10.23.4.22 Accelerometer and Seismometer, Elsevier. [Online] Available at: https://app.knovel.com/hotlink/pdf/id:kt00UCPLO1/treatise-geophysics-11/accelerometer-seismometer, Accessed on: 06-19-2018

A

Appendix 1

AK Steel **CARLITE® GRAIN ORIENTED ELECTRICAL STEELS**

SPECIFICATIONS

In terms of maximum core loss, AK Steel CARLITE Grain Oriented Electrical Steel specifications are determined at 15 kG and 17 kG at 60 Hz. Core loss grading is conducted using as-sheared single sheet test samples which are tested in accordance with ASTM test method A804. Peak permeability is specified at 10 Oe. Permeability grading is conducted using stress relief annealed Epstein samples tested in accordance with ASTM test method A343. Samples are secured from each end of the coil and the higher core loss and lower permeability values are used for certification of conformance to product grade guarantees.

GUARANTEED CORE LOSS AND LAMINATION FACTOR

Product Name	Approximate Equivalent ASTM Grades	Nominal Thickness, in. (mm)	Assumed Density, gm/cm³	Resistivity, Ω-m, x10⁻⁸	Maximum Core Loss Watts per pound				Minimum Peak Permeability at 10 Oe	Minimum Lamination Factor, %
					50 Hz		60 Hz			
					15 kG	17 kG	15 kG	17 kG		
M-3 CARLITE	23G045 23H070	0.009 (0.23)	7.65	51	0.340	0.530	0.445	0.700	1780	94.5%
M-4 CARLITE	27G051 27H074	0.011 (0.27)			0.390	0.560	0.510	0.740	1780	95.0%
M-5 CARLITE	30G058 30H083	0.012 (0.30)			0.440	0.630	0.580	0.830	1780	95.5%
M-6 CARLITE	35G066 35H094	0.014 (0.35)			0.500	0.710	0.660	0.940	1780	96.0%

TYPICAL CORE LOSS AND LAMINATION FACTOR

Product Name	Approximate Equivalent ASTM Grades	Nominal Thickness, in. (mm)	Assumed Density, gm/cm³	Resistivity, Ω-m, x10⁻⁸	Typical Core Loss Watts per pound				Typical Peak Permeability at 10 Oe	Typical Lamination Factor, %
					50 Hz		60 Hz			
					15 kG	17 kG	15 kG	17 kG		
M-3 CARLITE	23G045 23H070	0.009 (0.23)	7.65	51	0.304	0.457	0.394	0.585	1844	96.1%
M-4 CARLITE	27G051 27H074	0.011 (0.27)			0.351	0.518	0.460	0.670	1845	96.9%
M-5 CARLITE	30G058 30H083	0.012 (0.30)			0.390	0.566	0.513	0.736	1834	97.2%
M-6 CARLITE	35G066 35H094	0.014 (0.35)			0.440	0.627	0.582	0.823	1848	97.2%

The core loss and exciting power of the AK Steel TRAN-COR® H grades are determined by magnetic tests performed in accordance with general procedures approved by the American Society for Testing and Materials. The following conditions apply:
1. Results for as-sheared single sheet specimens from fully processed material cut parallel to the rolling direction of the coil and tested per ASTM A804
2. Density of all grades (7.65 gm/cm³) per ASTM A343
ASTM A664 is a grade identification system for electrical steels. While this system has not been widely adopted by the manufacturers and consumers of electrical steels, it is used in ASTM A876 to designate various grades of grain oriented electrical steel.

2

Figure A.1: Specification of the steel provided by the manufacturer

AK Steel **CARLITE®** GRAIN ORIENTED ELECTRICAL STEELS

TYPICAL VALUES OF CORE LOSS

AT 50 AND 60 Hz FOR TYPICAL SPECIMENS OF AK STEEL ORIENTED CARLITE COATED ELECTRICAL STEELS

Flux Density (kG)	Core Loss (W/lb) - ASTM A804 (Sheet Specimens)							
	0.009 in. M-3 Oriented CARLITE		0.011 in. M-4 Oriented CARLITE		0.012 in. M-5 Oriented CARLITE		0.014 in. M-6 Oriented CARLITE	
	50 Hz	60 Hz	50 Hz	60 Hz	50 Hz	60 Hz	50 Hz	60 Hz
1	0.00147	0.00192	0.00183	0.00242	0.00195	0.00259	0.00247	0.00329
2	0.00257	0.00742	0.00702	0.00928	0.00757	0.0101	0.00928	0.0124
3	0.0125	0.0163	0.0152	0.0202	0.0165	0.0220	0.0199	0.0267
4	0.0218	0.0285	0.0265	0.0347	0.0286	0.0381	0.0342	0.0458
5	0.0336	0.0438	0.0400	0.0528	0.0437	0.0580	0.0518	0.0694
6	0.0477	0.0621	0.0564	0.0742	0.0617	0.0819	0.0728	0.0973
7	0.0641	0.0834	0.0753	0.0990	0.0828	0.110	0.0971	0.130
8	0.0829	0.108	0.0968	0.127	0.107	0.142	0.125	0.166
9	0.104	0.135	0.121	0.159	0.134	0.178	0.156	0.208
10	0.128	0.166	0.148	0.195	0.165	0.218	0.191	0.254
11	0.154	0.200	0.179	0.236	0.199	0.263	0.230	0.305
12	0.183	0.238	0.214	0.281	0.238	0.314	0.273	0.363
13	0.217	0.282	0.253	0.333	0.281	0.371	0.322	0.427
14	0.255	0.331	0.298	0.391	0.330	0.435	0.376	0.498
15	0.303	0.393	0.353	0.462	0.390	0.513	0.440	0.582
16	0.363	0.467	0.418	0.546	0.462	0.605	0.517	0.683
17	0.455	0.581	0.514	0.666	0.566	0.736	0.625	0.823
18	0.609	0.773	0.658	0.845	0.719	0.930	0.776	1.02
19	0.795	0.999	0.770	0.990	0.898	1.15	0.921	1.19

Flux Density (kG)	Core Loss (W/lb) - ASTM A343 (Epstein Specimens)							
	0.009 in. M-3 Oriented CARLITE		0.011 in. M-4 Oriented CARLITE		0.012 in. M-5 Oriented CARLITE		0.014 in. M-6 Oriented CARLITE	
	50 Hz	60 Hz	50 Hz	60 Hz	50 Hz	60 Hz	50 Hz	60 Hz
1	0.00154	0.00201	0.00189	0.00249	0.00195	0.00260	0.00251	0.00334
2	0.00581	0.00762	0.00707	0.00935	0.0075	0.0100	0.00921	0.0123
3	0.0127	0.0167	0.0153	0.0202	0.0164	0.0219	0.0197	0.0265
4	0.0222	0.0291	0.0264	0.0346	0.0285	0.0381	0.0338	0.0453
5	0.0343	0.0447	0.0402	0.0531	0.0437	0.0582	0.0513	0.0687
6	0.0489	0.0636	0.0568	0.0748	0.0620	0.0823	0.0721	0.0964
7	0.0659	0.0858	0.0761	0.100	0.0833	0.111	0.0964	0.129
8	0.0854	0.111	0.0981	0.129	0.108	0.143	0.124	0.165
9	0.107	0.140	0.123	0.162	0.136	0.180	0.155	0.207
10	0.132	0.172	0.151	0.198	0.166	0.220	0.190	0.253
11	0.159	0.207	0.182	0.239	0.201	0.266	0.229	0.305
12	0.189	0.246	0.217	0.285	0.240	0.317	0.273	0.362
13	0.223	0.291	0.255	0.336	0.283	0.374	0.321	0.425
14	0.263	0.341	0.300	0.395	0.332	0.438	0.375	0.496
15	0.311	0.402	0.354	0.463	0.390	0.513	0.437	0.578
16	0.374	0.481	0.421	0.550	0.463	0.606	0.512	0.676
17	0.468	0.598	0.520	0.673	0.563	0.733	0.612	0.806
18	0.631	0.801	0.680	0.872	0.717	0.925	0.765	1.00
19	0.824	1.03	0.845	1.090	0.895	1.15	0.943	1.22

7

Figure A.2: Loss values of the steel provided by the manufacturer

AK Steel **CARLITE®** GRAIN ORIENTED ELECTRICAL STEELS

TYPICAL VALUES OF RMS EXCITING POWER

AT 50 AND 60 Hz FOR TYPICAL SPECIMENS OF AK STEEL ORIENTED CARLITE COATED ELECTRICAL STEELS

Flux Density (kG)	Exciting Power (rms VA/lb) - ASTM A804 (Sheet Specimens)							
	0.009 in. M-3 Oriented CARLITE		0.011 in. M-4 Oriented CARLITE		0.012 in. M-5 Oriented CARLITE		0.014 in. M-6 Oriented CARLITE	
	50 Hz	60 Hz	50 Hz	60 Hz	50 Hz	60 Hz	50 Hz	60 Hz
1	0.00458	0.00560	0.00472	0.00583	0.00418	0.00521	0.00406	0.00516
2	0.0152	0.0186	0.0154	0.0192	0.0138	0.0174	0.0134	0.0173
3	0.0300	0.0369	0.0305	0.0381	0.0275	0.0348	0.0270	0.0350
4	0.0479	0.0592	0.0488	0.0613	0.0447	0.0567	0.0443	0.0576
5	0.0683	0.0846	0.0699	0.0881	0.0650	0.0827	0.0651	0.0848
6	0.0910	0.113	0.0937	0.118	0.0882	0.112	0.0893	0.116
7	0.116	0.144	0.120	0.152	0.114	0.147	0.117	0.153
8	0.143	0.179	0.149	0.189	0.144	0.185	0.148	0.193
9	0.173	0.217	0.181	0.231	0.177	0.228	0.183	0.239
10	0.207	0.259	0.218	0.277	0.215	0.276	0.222	0.290
11	0.244	0.306	0.258	0.329	0.258	0.331	0.266	0.348
12	0.288	0.360	0.306	0.389	0.309	0.396	0.318	0.414
13	0.343	0.429	0.365	0.463	0.372	0.476	0.379	0.493
14	0.410	0.511	0.437	0.553	0.456	0.580	0.456	0.591
15	0.521	0.645	0.552	0.694	0.582	0.733	0.571	0.734
16	0.687	0.843	0.711	0.883	0.783	0.975	0.761	0.965
17	1.20	1.45	1.25	1.53	1.45	1.78	1.38	1.71
18	3.19	3.84	3.50	4.25	4.11	4.99	4.16	5.01
19	11.7	14.1	12.4	15.1	13.8	16.8	15.2	18.2

Flux Density (kG)	Exciting Power (rms VA/lb) - ASTM A343 (Epstein Specimens)							
	0.009 in. M-3 Oriented CARLITE		0.011 in. M-4 Oriented CARLITE		0.012 in. M-5 Oriented CARLITE		0.014 in. M-6 Oriented CARLITE	
	50 Hz	60 Hz	50 Hz	60 Hz	50 Hz	60 Hz	50 Hz	60 Hz
1	0.00413	0.00504	0.00424	0.00524	0.00398	0.00496	0.00393	0.00499
2	0.0139	0.0171	0.0141	0.0176	0.0135	0.0171	0.0132	0.0169
3	0.0279	0.0343	0.0283	0.0354	0.0274	0.0347	0.0267	0.0346
4	0.0449	0.0555	0.0457	0.0574	0.0448	0.0569	0.0440	0.0572
5	0.0645	0.0799	0.0659	0.0831	0.0652	0.0831	0.0648	0.0844
6	0.0862	0.107	0.0887	0.112	0.0887	0.113	0.0889	0.116
7	0.110	0.137	0.114	0.145	0.115	0.147	0.116	0.152
8	0.136	0.170	0.142	0.181	0.145	0.186	0.147	0.193
9	0.165	0.206	0.173	0.221	0.178	0.229	0.182	0.238
10	0.196	0.246	0.208	0.265	0.215	0.277	0.221	0.288
11	0.232	0.291	0.248	0.316	0.259	0.332	0.264	0.345
12	0.274	0.343	0.294	0.374	0.309	0.396	0.314	0.409
13	0.325	0.406	0.351	0.445	0.371	0.474	0.372	0.484
14	0.392	0.489	0.424	0.537	0.452	0.575	0.444	0.575
15	0.494	0.612	0.533	0.669	0.572	0.722	0.544	0.699
16	0.683	0.839	0.726	0.901	0.788	0.980	0.713	0.904
17	1.17	1.41	1.24	1.52	1.34	1.65	1.16	1.43
18	3.24	3.90	3.72	4.52	3.76	4.57	3.43	4.13
19	14.7	17.7	16.4	20.0	14.7	18.0	14.4	17.2

8

Figure A.3: Excitation power required as per the manufacturer

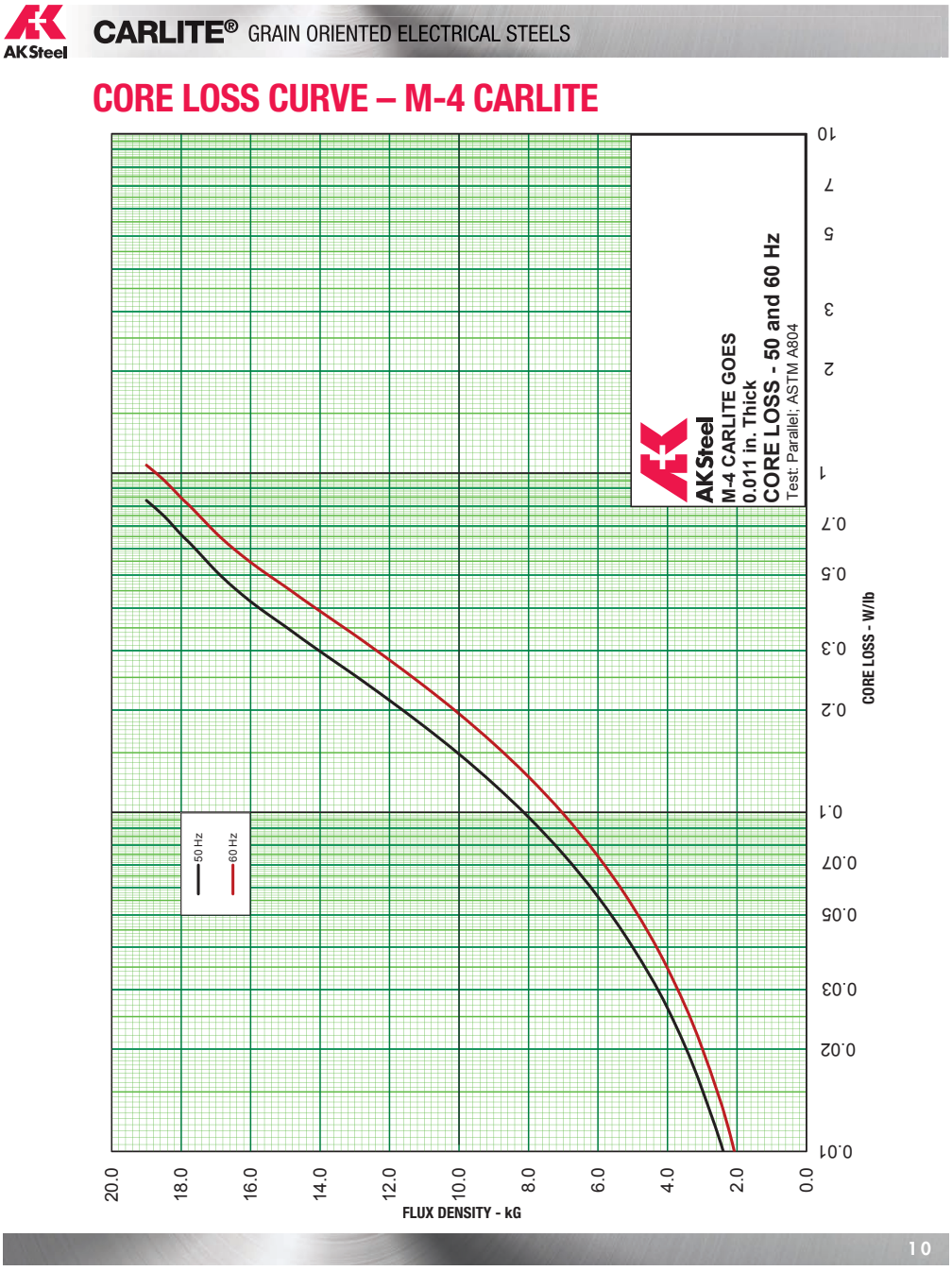

Figure A.4: Loss curve of the steel provided by the manufacturer

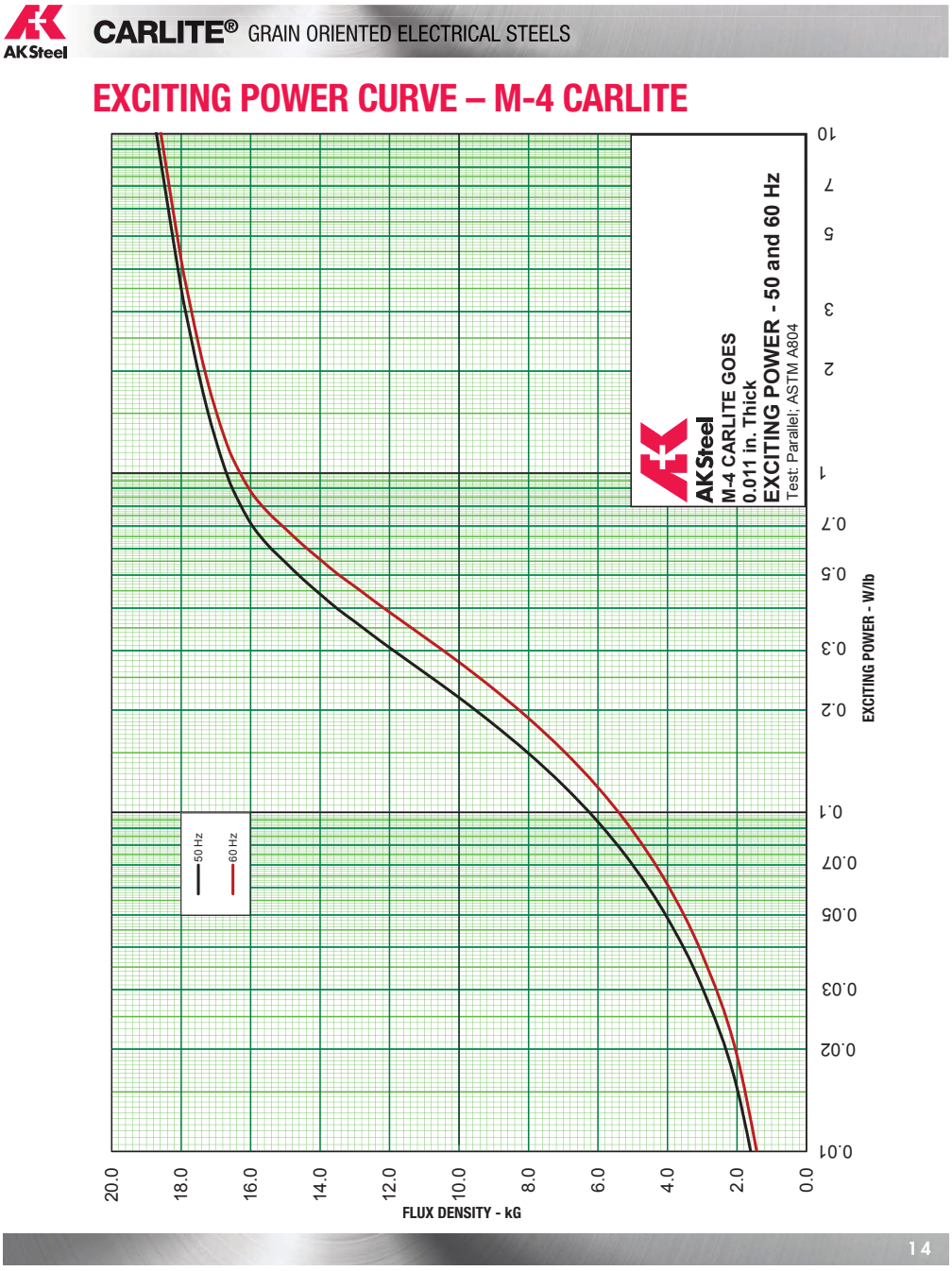

Figure A.5: Excitation power curve of the steel provided by the manufacturer

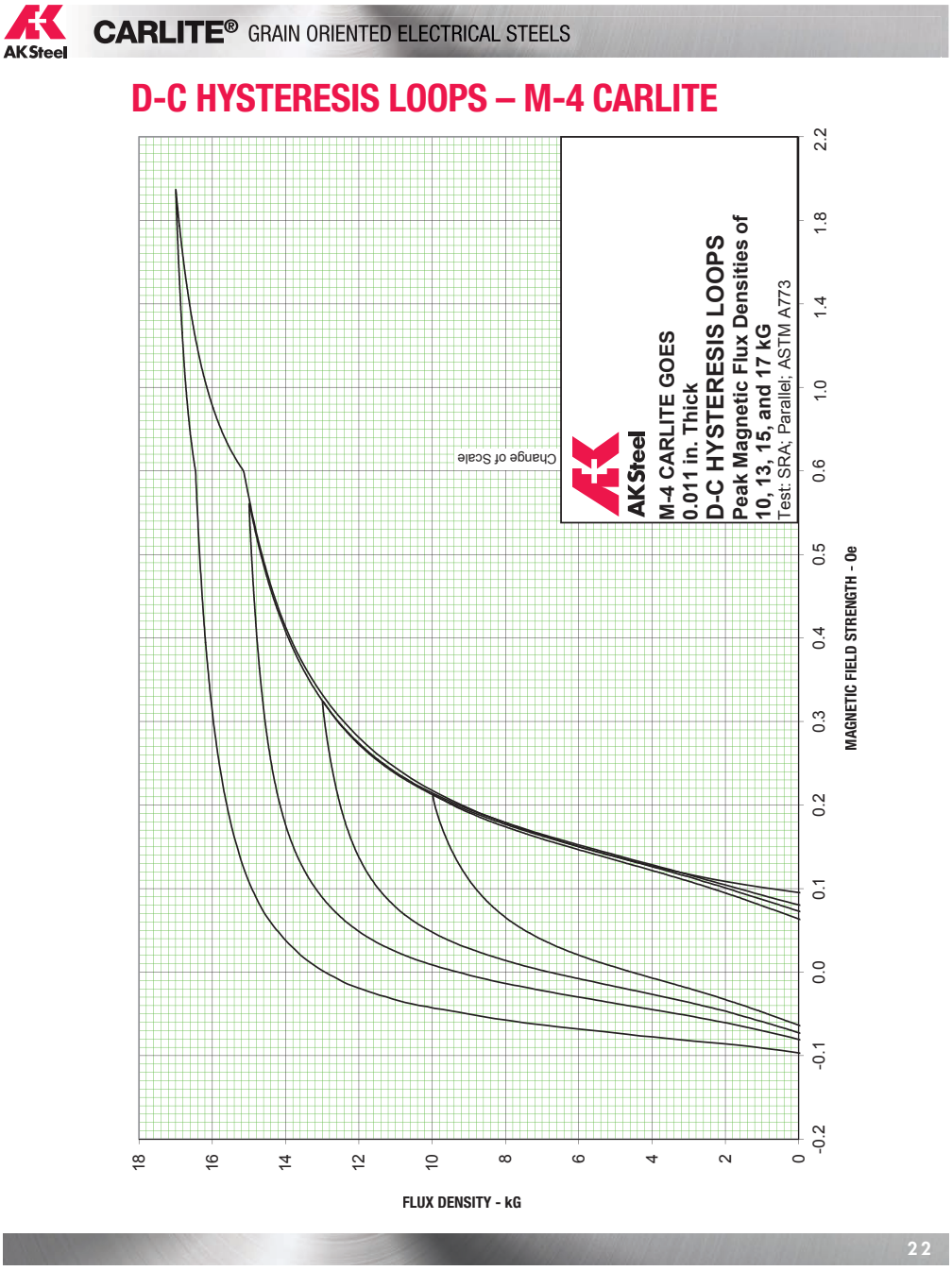

Figure A.6: DC hysteresis loop of the steel provided by the manufacturer